Theses and Dissertations 1. Thesis and Dissertation Collection, all items

1989

Bubble production by breaking waves

Daniel, Albert C., Jr.

Monterey, California. Naval Postgraduate School

http://hdl.handle.net/10945/26903

NAVAL POSTGRADUATE SCHOOL
Monterey, California

THESIS

D147742

BUBBLE PRODUCTION BY BREAKING WAVES

by

Albert C. Daniel Jr.

December 1989

Thesis Advisor   Herman Medwin

Unclassified
security classification of this page

<div align="center">

REPORT DOCUMENTATION PAGE

</div>

1a Report Security Classification Unclassified			1b Restrictive Markings			
2a Security Classification Authority			3 Distribution Availability of Report			
2b Declassification Downgrading Schedule			Approved for public release; distribution is unlimited.			
4 Performing Organization Report Number(s)			5 Monitoring Organization Report Number(s)			
6a Name of Performing Organization Naval Postgraduate School		6b Office Symbol (if applicable) 33	7a Name of Monitoring Organization Naval Postgraduate School			
6c Address (city, state, and ZIP code) Monterey, CA 93943-5000			7b Address (city, state, and ZIP code) Monterey, CA 93943-5000			
8a Name of Funding Sponsoring Organization		8b Office Symbol (if applicable)	9 Procurement Instrument Identification Number			
8c Address (city, state, and ZIP code)			10 Source of Funding Numbers			
			Program Element No	Project No	Task No	Work Unit Accession No
11 Title (include security classification) BUBBLE PRODUCTION BY BREAKING WAVES						
12 Personal Author(s) Albert C. Daniel Jr.						
13a Type of Report Master's Thesis	13b Time Covered From To		14 Date of Report (year, month, day) December 1989		15 Page Count 63	
16 Supplementary Notation The views expressed in this thesis are those of the author and do not reflect the official policy or position of the Department of Defense or the U.S. Government.						

17 Cosati Codes			18 Subject Terms (continue on reverse if necessary and identify by block number)
Field	Group	Subgroup	Bubble production density

19 Abstract (continue on reverse if necessary and identify by block number)

It has been shown (Medwin and Beaky, J. Acoust. Soc. Am., v. 86, 1124-1130 (1989)) that spilling breakers in the laboratory produce a sound close to the Knudsen sea surface noise spectrum from 400 Hz to 20 kHz. The surface spectral production density of newly-created near surface bubbles under these laboratory spilling breakers has now been acoustically determined by using an array of hydrophones. The surface spectral density has been obtained by identifying the individual bubbles that create this noise spectrum. The radii were calculated from the resonance frequencies. The bubble positions on the surface of the water were determined from the difference in time of arrival of the bubble radiation to the elements of two vertical arrays of hydrophones. The production area and rate of production of bubbles of radii 0.048 to 7.40 millimeters have been calculated and the total volume of air encapsulated into bubble foam per unit area of spilling breakers has been determined.

20 Distribution Availability of Abstract ☒ unclassified unlimited ☐ same as report ☐ DTIC users	21 Abstract Security Classification Unclassified	
22a Name of Responsible Individual Herman Medwin	22b Telephone (include Area code) (408) 646-2385	22c Office Symbol 61MD

DD FORM 1473,84 MAR   83 APR edition may be used until exhausted   security classification of this page
All other editions are obsolete

<div align="right">Unclassified</div>

Bubble Production by Breaking Waves

by

Albert C. Daniel Jr.
Lieutenant, United States Navy
B.S., University of South Carolina, 1984

Submitted in partial fulfillment of the
requirements for the degree of

MASTER OF SCIENCE IN ENGINEERING ACOUSTICS

from the

NAVAL POSTGRADUATE SCHOOL
December 1989

ABSTRACT

It has been shown (Medwin and Beaky, J. Acoust. Soc. Am., v. 86, 1124-1130 (1989)) that spilling breakers in the laboratory produce a sound close to the Knudsen sea surface noise spectrum from 400 Hz to 20 kHz. The surface spectral production density of newly-created near surface bubbles under these laboratory spilling breakers has now been acoustically determined by using an array of hydrophones. The surface spectral density has been obtained by identifying the individual bubbles that create this noise spectrum. The radii were calculated from the resonance frequencies. The bubble positions on the surface of the water were determined from the difference in time of arrival of the bubble radiation to the elements of two vertical arrays of hydrophones. The production area and rate of production of bubbles of radii 0.048 to 7.40 millimeters have been calculated and the total volume of air encapsulated into bubble foam per unit area of spilling breakers has been determined.

TABLE OF CONTENTS

LIST OF FIGURES

ACKNOWLEDGEMENT

I. INTRODUCTION

The purpose of this thesis is to develop a method for the determination of the bubble production density from breaking waves. The motivation for this study came from the observation that the spectrum produced from the noise of the breaking waves in the laboratory tank at the Naval Postgraduate School closely resembled the Knudsen sea surface spectrum of the ambient noise at sea. This development suggested that the breaking waves experimentally produced will exhibit the same bubble characteristics as breaking waves at sea. It is hoped that the capability of comparing the calculated bubble production density with the area of foam coverage monitored with satellite imaging and aerial photography will aid in acoustical and meteorological research of air/sea interactions by predicting the number and size of bubbles which may be found in the region being studied.

The method used in this research is to utilize passive acoustics to identify individual bubbles created from breaking waves. The breaking of the wave, characterized by the initial formation of a large amplitude, low frequency bubble, was used as a triggering source for the signal processing equipment. The location of each subsequent bubble was calculated by using the difference in time of arrival of the noise from the bubble to the different elements of a hydrophone array. The bubble production area can be measured by positioning all the bubble locations on a grid. The rate of bubble production was observed to behave as an exponentially decreasing function of time. This was determined by noting the relative time of arrival of the pressure waves from the individual oscillating bubbles to a hydrophone array. The bubble production density and volume rate of gas entrainment were calculated from the bubble population data and the measured area of bubble production. This technique provided information on bubble production on the surface, a quantity which had not been directly measured in any other previous experimental work.

1

II. BACKGROUND

Many processes of acoustical, meterological, geochemical, and biological interest are associated with the presence of bubbles in the near surface of the oceans. Among these are ambient noise, aerosol formation, surface coagulation, fractionalization of organic or inorganic materials, and gas exchange. The bubble populations that influence these phenomena are composed of bubble patches produced by breaking waves superimposed on a background population of bubbles.

The background population of bubbles originates from bubble patches due to previous breaking waves, biological activity, droplet impacts, and sediment outgassing. Some of these bubbles will rise and eventually burst on the surface affecting the processes already mentioned. Other bubbles undergo diffusion and will completely dissolve. An expression given by Levich (1962) for the rate at which these bubbles will dissolve is described by the following equation:

$$\frac{dn}{dt} = -7.98 D^{\frac{2}{3}} u^{\frac{1}{3}} a^{\frac{4}{3}} C$$

where n is the number of moles of the gas, D is the gas diffusivity in $m^2/$ sec , u is the bubble velocity in m sec, a is the bubble radius in meters, and C is the Peclet number which describes diffusive mass transfer.

The vertical distribution of the bubbles beneath the surface has been studied by Thorpe (1986) and Farmer and Vagle (1989). Clouds of subsurface bubbles caused by wind waves breaking in deep water and creating whitecaps have been observed using a vertically pointing narrow beam sonar and a dual beam side scanning sonar. The vertical distribution of bubbles is influenced by several actions: the turbulent transport from a source at the surface, the rise of the bubbles due to buoyancy, the change in bubble radius due to the diffusion discussed earlier, and change of hydrostatic pressure. The turbulence includes the forces from the whitecaps, the shear from the breaking wave, internal waves, and Langmuir circulation. Thorpe's equation representing the process is

$$-w_b \frac{dN}{dz} = K_v \frac{d^2 N}{dz^2} - \sigma N$$

Where w_b is the rising velocity of the bubbles in m/sec, N is the number of bubbles per unit volume, K_v is the turbulent diffusion coefficient in $m^2/$ sec , and σ is the bubble loss rate due to diffusion in number of bubbles per second.

There have been many other techniques developed to measure these background bubbles. Johnson and Cooke (1979) and Toba (1961) utilized a photographic method to accomplish this task. Three images corresponding to the specular reflections of the light provided by three strobes served to identify bubbles and as the basis for measurement. The depth of field was established by the intersection of three dots and a high resolution film allowed a 3X magnification. This method claimed identification of bubbles with radii as small as 17 μm. The procedure requires the water to be in a clean, clear chute and can identify bubble radii with only poor resolution. The abundance of debris and other matter would interfere with accurate identification of bubbles with a radius of less than 0.1 mm. Kolovayev (1976) used a bubble trap in order to concentrate the bubbles to allow measurements by photographic means. Breitz and Medwin (1989) developed a floating acoustical resonator to determine the number and size of bubbles produced from spilling breakers at sea. The Q of the resonator was changed by bubble presence. The system allowed measurement of bubble populations of nine radii between 30 and 270 μm. Though accurate, this method measured bubbles at a depth of 25 cm below the surface and getting densities at a shallower depth may not be possible.

With these successful results in measuring and understanding the background bubbles, the next major area for study is to examine the origins of the bubbles and the relationships between these bubble producing actions.

A large proportion of bubbles in the oceans originate from the whitecaps of breaking waves. Holthuijsen and Herbers (1986) conducted measurements of wave height, period, steepness, crest front steepness, horizontal crest asymmetry, and vertical crest asymmetry, in an attempt to estimate from these parameters the likelihood that a wave will break. They concluded that breaking waves cannot be separated from non-breaking waves with these factors. Thorpe and Hall (1983) arrived at several conclusions from observations of waves at sea: separate bubble clouds are created by individual waves; the breaking crests are seldom more than several meters long; waves generally continue to break as they advance so the horizontal size of the bubble clouds increases with wind speed. Another mechanism of bubble production involves the small capillary waves that can be observed on that front face of long gravity waves even in the absence of wind. These capillary waves can break and pinch off air bubbles in the same manner as the breaking gravity waves.

The role of surface tension in breaking waves is also important. Miller (1972) performed a series of experiments on lowering the surface tension of the water with chemicals. In these experiments it was found that, as the surface tension decreased, the waves got higher before they broke. Gucinski (1986) found that the persistence of visible bubbles at sea is longer than that in fresh water during similar wind and sea conditions. A contributing factor is the presence of organic matter which surrounds the bubble interfaces. Laboratory experiments show an increasing coalescence with increasing ionic strengths.

Since distributions of wind and wind waves can be collected by satellite sensors, the development of expressions for related phenomena as functions of these winds and waves should be useful. Many studies have been made and great quantities of data have been taken of wind stress and whitecap coverage measured from a level of 10 meters. Toba and Koga (1968) have shown that the percentage of breaking waves (α), percentage of whitecap coverage (P), and the concentration of sea salt particles (Θ), are related by the following term:

$$\alpha = 4.3 x 10^{-3} \frac{u_{\times}^2}{v\sigma}$$

$$P = 8.9 x 10^{-5} \frac{u_{\times}^2}{v\sigma}$$

$$\Theta = 65 \frac{u_{\times}^2}{v\sigma}$$

where $u_{\times}$ is the surface friction velocity of air in m sec, v is the kinematic viscosity of air in $m^2/$ sec , and σ is the spectral peak frequency of the wind waves. It is now also possible to measure the tropospheric aerosols over the oceans with satellites. The method relates the upwelling visible radiants measured by the satellite to the aerosol optical thickness of the atmosphere. There is a relationship between the radiance and the aerosol optical thickness which varies with parameters such as aerosol size, distribution, and refractive index. The correlation between the sources of the aerosols, such as breaking waves and bursting bubbles, and their concentration in the atmosphere is still not understood.

The use of passive acoustics and modern signal processing allows individual bubbles to be examined as they are created by the breaking wave. Medwin and Beaky (1989) separated the characteristics of these bubbles into four distinct categories. These

categories describe the bubble damping, resonance frequency, and oscillation patterns. With the method described in this thesis, utilizing the same equipment as Medwin and Beaky, the location of these individual bubbles can be determined from the geometry of the hydrophone array and the difference in the time of arrival of the pressure field to the individual elements. From this data the exponentially decreasing temporal rate of bubble creation from an individual breaking wave can be calculated, as well as the production density in bubbles per unit area originating from a single breaking wave. The volume of gas encapsulation per unit surface area of a spilling breaker can be computed from the bubble density. This could be useful in studies of gas exchange at the ocean surface.

If all the information and methods described can be integrated and successfully utilized it will be possible to obtain a complete perspective on the generation of bubbles at sea. The background bubbles are understood and can be measured; the main source of bubble creation, particularly whitecap coverage from breaking waves, can be estimated; the physical and chemical makeup of the water can be examined; and now with the use of the method described in this thesis it is possible to predict the rate of bubble production from the whitecaps. This information, when combined, will further aid in our understanding the effect of air/sea interaction on our environment.

III. FACILITIES AND APPARATUS

The laboratory facilities include a 57x4x4 foot wave tunnel emptying into a 10x10x10 foot anechoic tank. A motor-driven reciprocating wedge generates the waves at the beginning of the tunnel. The waves break approximately three feet after entering the tank. The exact position of where the waves will break was not controlled. The tank sides and bottoms are lined with Redwood pilings. After spilling, the waves are absorbed by a "beach" consisting of an aluminum shavings wedge which minimizes the wave reflection at the tank boundary.

Medwin and Beaky (1989) conducted tests in the tank which demonstrated at least a 15 decibel difference between a signal and the strongest reflection from the tank walls at frequencies under 5 kHz, and at least 20 dB at frequencies above 5 kHz, when the hydrophone is 24 cm from the bubble source. The signal to reverberant noise ratio is better for shallower hydrophones.

Two vertical arrays of 2 omnidirectional hydrophones with the shallow hydrophone at a depth of 15 cm and the deep hydrophone at a depth of 31 cm are situated in the approximate area where the majority of the waves break as depicted in figure (1). The output signals are input into an Ithaco 1250 voltage amplifier bandpass filter with the bandpass frequencies set between 300 Hz and 100 kHz. The amplifier output splits into a Hewlett-Packard 3561A signal analyzer and also into an IBM XT personal computer with an R. C. Electronics "computerscope" analog to digital converter. The signal analyzer and the "computerscope" allow the operator to select triggering level. The signal analyzer triggers at an input level of 0.837 Volts which, for an amplification of 5000, corresponds to an acoustic pressure of 1.4 Pascals.

This "computerscope" analog to digial conversion software package samples the data with a sampling period of 1 microsecond with one input, 2 microseconds with two inputs, and accordingly, 4 microseconds with four inputs with a 12 bit amplitude resolution. The sampled signal is displayed both graphically and numerically with curser movement. The buffer is 64 milliseconds long with the minimum sampling period of 1 microsecond and can be lengthened by a corresponding increase in the sampling period. Sections of the buffer can be "expanded" or "compressed" in time and the amplitude of

the signal display can also be adjusted. This enables the user to manipulate the graphical presentation to obtain a signal that can be accurately analyzed and also to adjust the sampling rate to maximize the signal resolution.
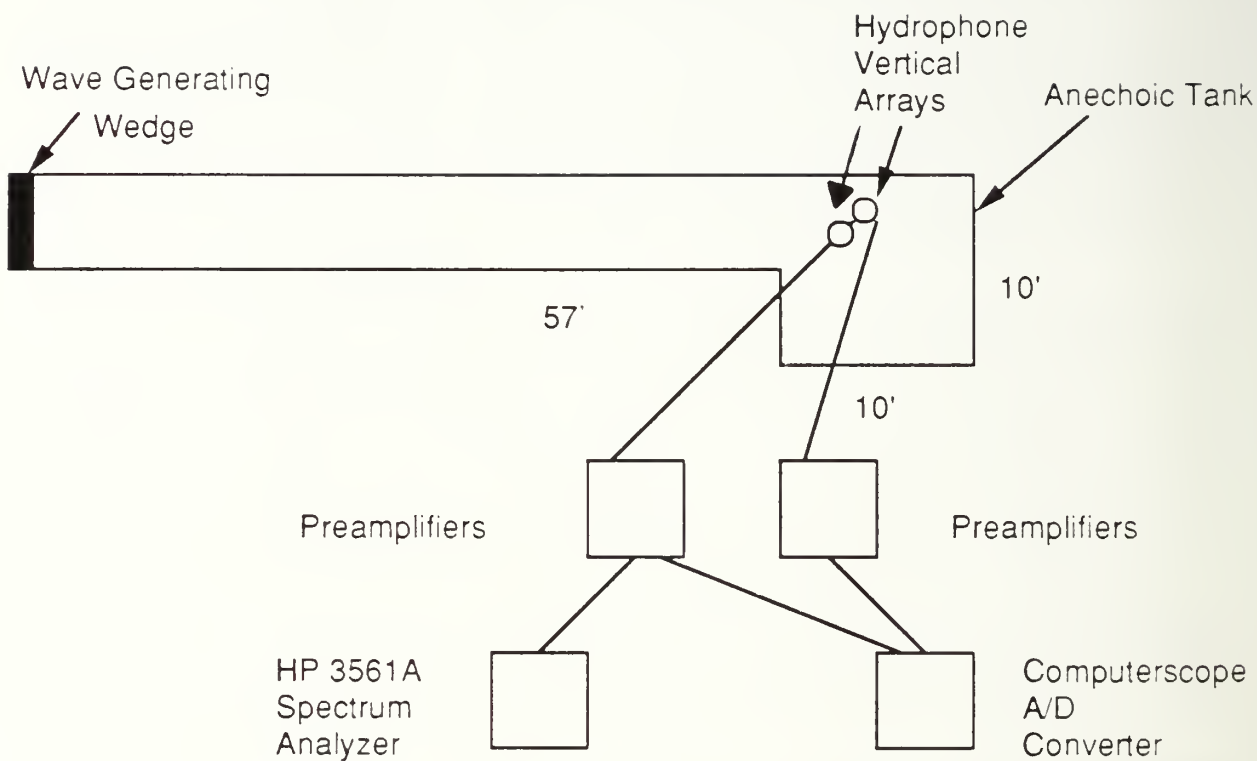
Figure 1.   Equipment setup.

8

IV. EXPERIMENT

A. BREAKER SPECTRUM

During World War II many observations of the ambient noise of the oceans showed that "wind noise" is the primary source of the noise in the frequency range between 500 Hz and 20 kHz. The famous Knudsen spectra broke down this large collection of data in a manner intended to demonstrate the wind speed dependence of the noise level. This spectrum is reproduced from Urick (1983) as figure (2). The possible processes, as given by Urick, which produced this noise were hypothesized to be "crash noises of breaking waves", "flow noise" produced by wind moving over the water, "cavitation noise", and "wave generating actions" of the wind. The paper by Medwin and Beaky (1989) proves that the catastrophically created, damped bubbles, by themselves, explain the Knudsen spectra. The slope of the noise spectrum in this frequency band is approximately -5 to -6 dB per octave or -17 dB per decade with the level increasing with wind speed. The noise in the frequencies outside this band was believed by Urick to originate from sources not directly dependant on wind speed such as shipping below 500 Hz and thermal noise above 50 kHz.

In order to determine the noise spectrum of the waves breaking in the tank it was first necessary to ensure that the wave generating equipment was not acting as an additional noise source. Figure (3) shows the background ambient noise of the tank with no equipment in operation plotted with a dashed line. The ambient noise in the tank with the plunger in operation but no waves breaking is plotted with a solid line. Both plots were generated on the HP 3561A spectrum analyzer using a time average of 300 input signals, each of 500 milliseconds duration. The signal level was computed for frequencies between 500 Hz and 50 kHz.

The breaker spectrum was also obtained using the HP 3561A with the input from an omnidirectional hydrophone at a depth of 24 cm. The signal was divided into 40 sequential records, each of 20 millisecond duration. Each 20 millisecond band was Fourier transformed to provide the power for each 50 Hz block of the buffer."[6] The energy in these bands was summed only if the energy was 3 dB above the noted ambient noise level of the tank with no activity. This was done to ensure that the energy originated only from breaking waves in the tank. The breaking of a wave can usually be identified by a relatively high amplitude low frequency bubble which served as the triggering source

for the signal analyzer. The frequencies that were observed were restricted by the spectrum analyzer to between 400 Hz and 20 kHz. A total of six breaking waves was measured and the levels averaged. The results are displayed in figure (4). The slope of the spectrum is similar to the Knudsen spectra at approximately -17 dB per decade. The noise level at a frequency of 1 kHz is approximately 82 dB re $1\mu Pa^2/Hz$ which is somewhat greater than that of the Knudsen spectra at that frequency at high wind speeds. This is due to the laboratory measurements being made only when and where bubbles are being produced; a comparable situation at sea would require breaking waves to exist everywhere at all times as discussed by Medwin and Beaky (1989). The low noise level of figure (3) confirmed that the only significant sources that contribute to the sound levels above the ambient room noise are breakers produced by wave actions and not mechanical equipment. It should be observed that this phenomenon was observed under the condition of no wind over the tank. This confirms the suspicion that the actual source of the ambient noise are the breaking waves and not the wind. It was the fascinating fact that the spectrum in the tank is very similar to the expected spectrum in the oceans that convinced the author that the data produced by this study may be of future use to actual operations performed at sea. The method of using wind speed as a reference is useful, however, because the wind speed can be more dependably measured than the sea state. An interesting thing to note about the breaker spectrum is that below 1 kHz the level remains constant to the minimum frequency measured at 400 Hz.

M. S. Longuet-Higgins predicted that certain frequencies would be predominant from bubbles produced by breaking waves. These frequencies originate from modal distortions in the shape of the bubble during its creation. The frequencies were stated in a submitted paper, Longuet-Higgins (1989), to be at 1.38, 1.69, 2.10, 2.60, 3.32, 4.31, 5.70, 7.94, 11.4, and 16.8 kHz. These frequencies are designated by triangles on figure (4). The laboratory spectrum showed a peak only at two of these frequencies, 1.69 and 2.60 kHz. Several of the other frequencies correspond to the position of a minimum on the spectrum. This does not allow a determination of the significance of this phenomenon.
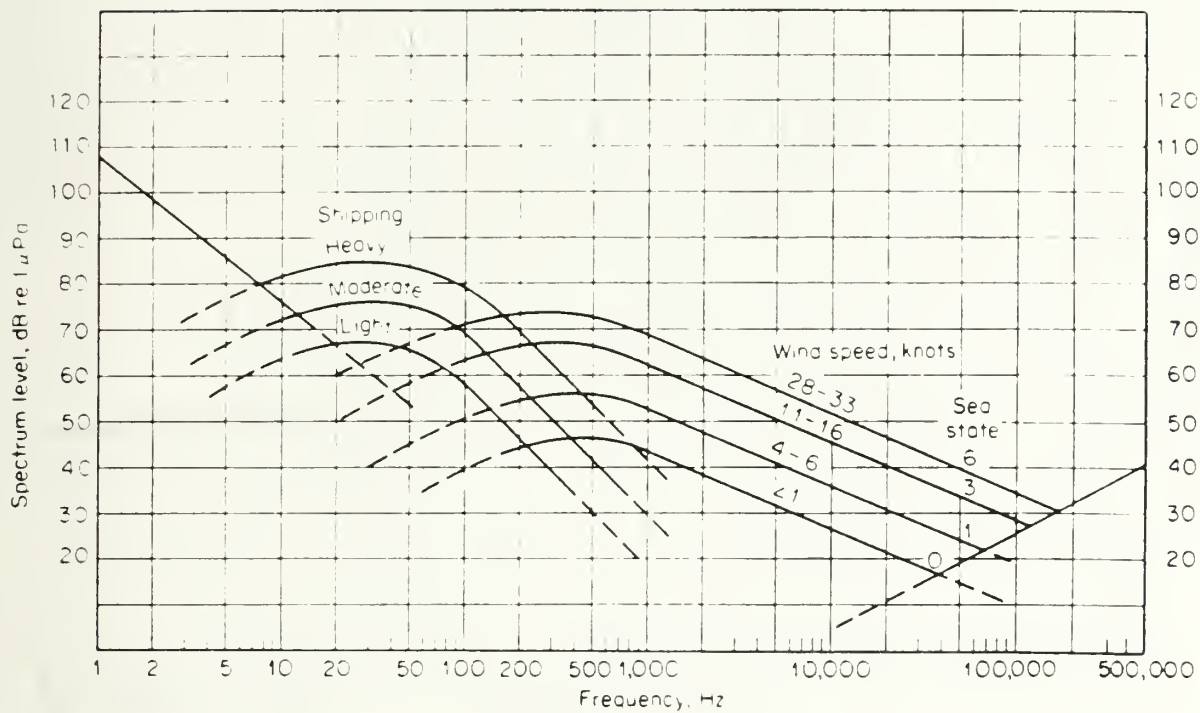
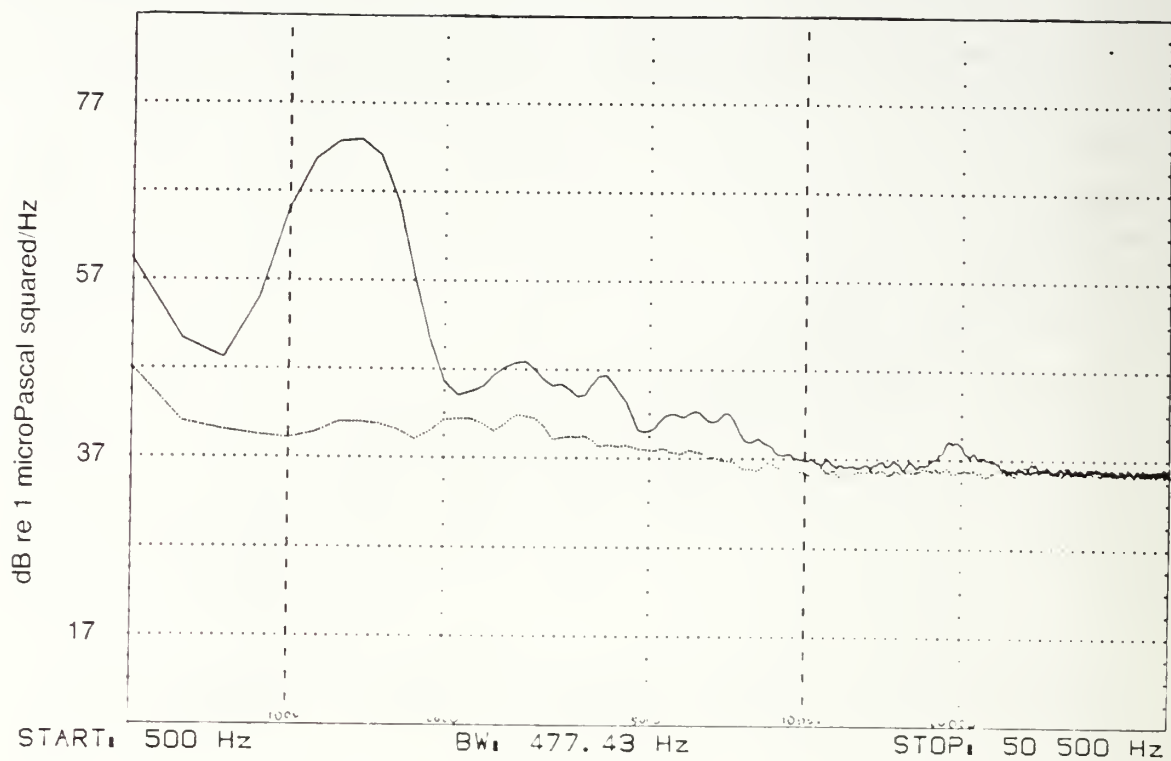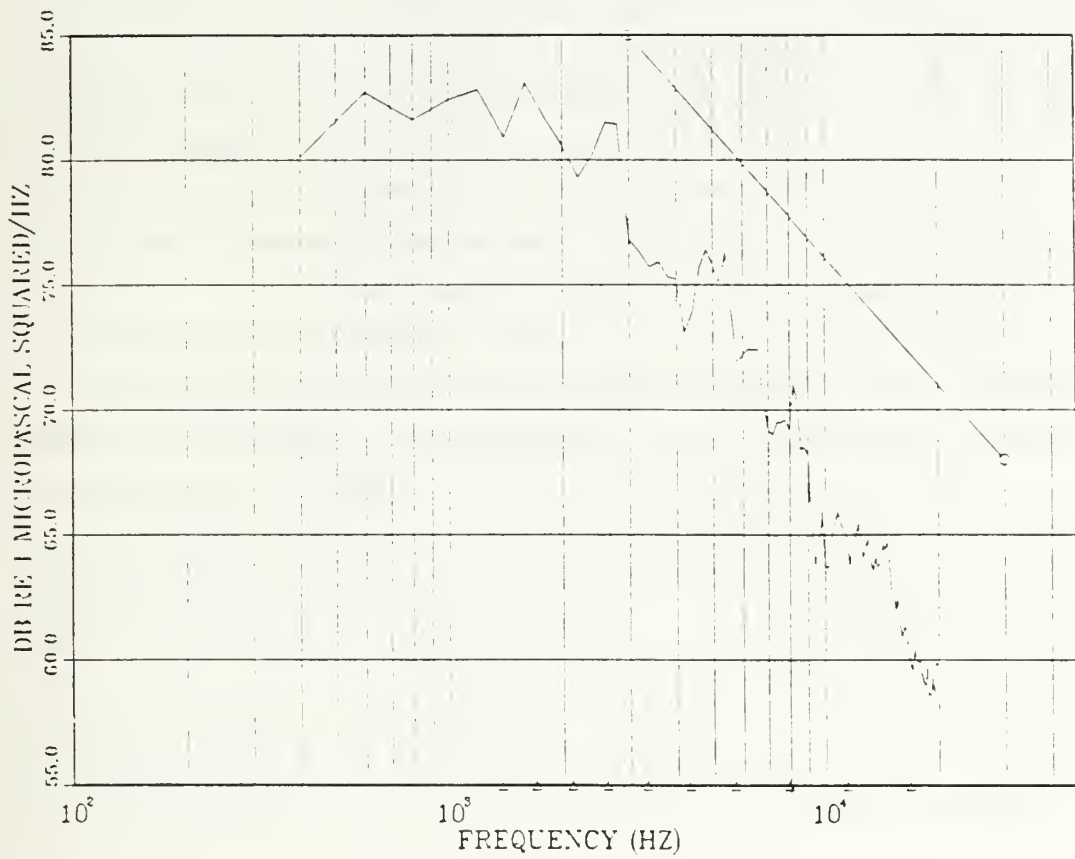Figure 2. Average deepwater ambient noise spectra. (Urick)

11

Figure 3. Anechoic tank background noise spectra: Solid line. plunger operating but no breakers. Dashed line. plunger off.

Figure 4. **Average noise spectrum from six breaking waves:** Triangles mark the
frequency peaks predicted by Longuet-Higgins. (1989)

13

B. BUBBLE IDENTIFICATION

It is possible to positively identify individual bubbles within the sound originating from the breaking of a wave. The equipment utilized is a hydrophone, a preamplifier, and an IBM XT personal computer with an R.C. Electronics Computerscope analog to digital converter. The converter samples the signal and allows detailed viewing of the desired segments of the captured noise.

When a wave breaks or "spills" air is entrained, bubbles are formed, and the bubbles oscillate to become sources of noise. In every wave observed with the signal processing equipment, the moment when the wave breaks can be identified by a large amplitude, low frequency bubble, with sufficient energy to be used as the triggering source for the signal analyzing equipment.

This equipment has already been used by Medwin and Beaky (1989) to characterize the bubbles from breaking waves by identifying the damping and modulation aspects most commonly observed. Four distinct bubble scenarios were classified: spherical bubbles with either a constant decay rate or with two different decay rates, a damped oscillation bubble appearing to shed a much smaller bubble, a near surface bubble which has an increasing amplitude as it moves away from the surface due to an increase in the dipole axis, and a bubble undergoing amplitude modulation possibly due to another bubble in close proximity with a slightly different frequency.

The resonance frequency of the bubbles was converted to bubble radius using the following relationship from Clay and Medwin (1977):

$$f = (\frac{1}{2\pi a})(\frac{3\gamma P}{\rho})^{\frac{1}{2}}$$

where f is the resonance frequency of the bubble in Hz, a is the bubble radius in meters, γ is the ratio of specific heats of the gas in the bubble, P is the hydrostatic pressure in N/m^2, and ρ is the density of the water in kg/m^3.

The large amplitude initial bubble created by a breaking wave can be seen in figure (5). This is the first 120 milliseconds of a 500 millisecond buffer. In this printout the upper and lower signals are from a hydrophone at 16 cm depth and a hydrophone at 31 cm depth respectively. The output signals are 180 degrees out of phase because of the amplifier output phase difference. The confirmation that it is indeed a bubble can be made from the damping relationship from Medwin and Beaky (1989)

$$\tau = \frac{1}{\pi f \delta}$$

where τ is the decay time in seconds to $1/e$ of its amplitude, f is the resonance frequency in Hertz, and δ is the damping constant. The measured frequency of the bubble in figure (5) is 505 Hz and the measured $1/e$ decay time is 30.9 milliseconds. From the table on page 199 of Clay and Medwin (1977) the damping constant for this frequency should be approximately 0.022. If placed in the above equation this damping constant yields a $1/e$ decay time of 28.6 milliseconds, a difference from the measured value of 7 percent. This is close enough to the theoretical value to ascertain that the bubbles are behaving as expected. If the presentation is expanded and viewed with more detail as in figure (6), additional later signals from higher frequency, smaller amplitude bubbles can be seen superimposed on the low frequency bubble signal. Finally, the presentation can be expanded even further, figure (7), to enable the accurate identification of a smaller bubble with frequency 16.6 kHz (196 micron radius) and accurate measurement of the difference in time of arrival of the signal to the individual hydrophones.

It can be seen in the above figures that the individual bubbles can be identified with enough resolution to obtain accurate information about bubble frequency, amplitude, and relative time of arrival at the hydrophones. The signal data was recorded only if a bubble could be confidently identified above any noise which may have been received. With this equipment accurate identification could be ensured if the signal level was at least 3 decibels above the measured ambient noise level of 37 dB re $1\mu Pa^2/Hz$ at the hydrophones. The resulting bubble count is thereby a conservative measure of the number of bubbles and would not include any bubbles with received signal less than the limit of 37 dB.
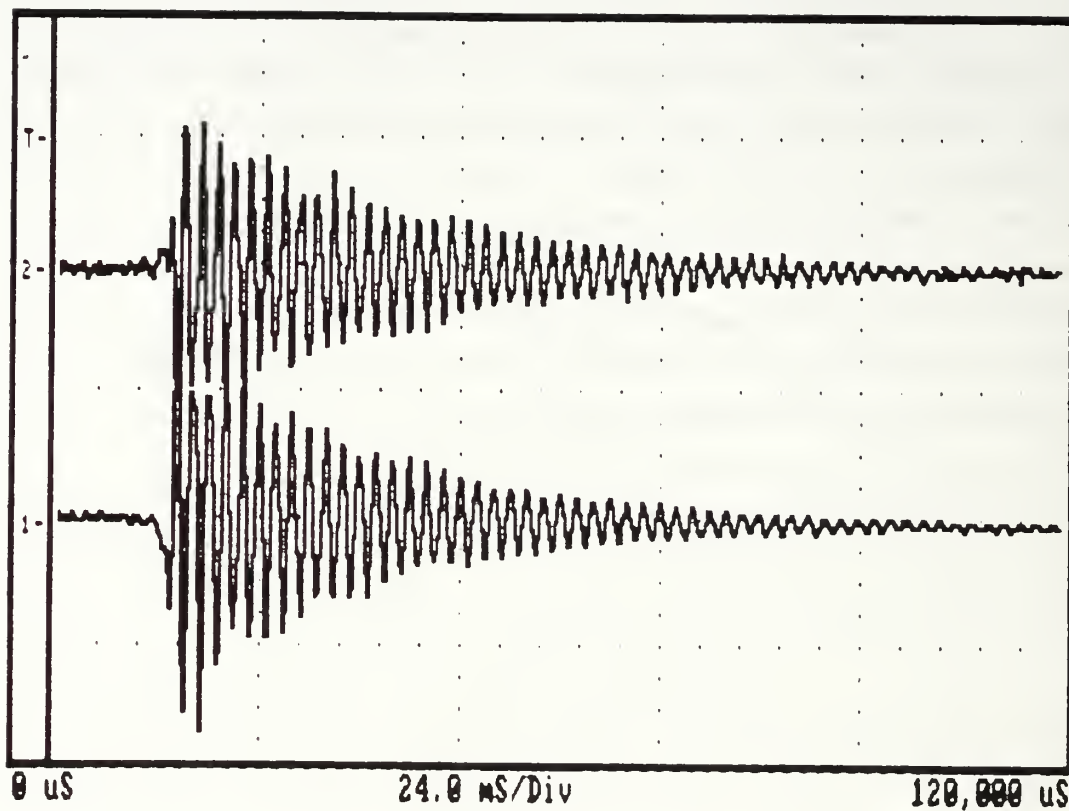
Figure 5. **Large triggering bubble from breaking wave:** Predominantly large
amplitude and low frequency bubble (505 Hz). Signal presentation is 120
ms. Outputs from two hydrophones shown. One output is inverted by the
amplifier. Sampling period is 15 microseconds.
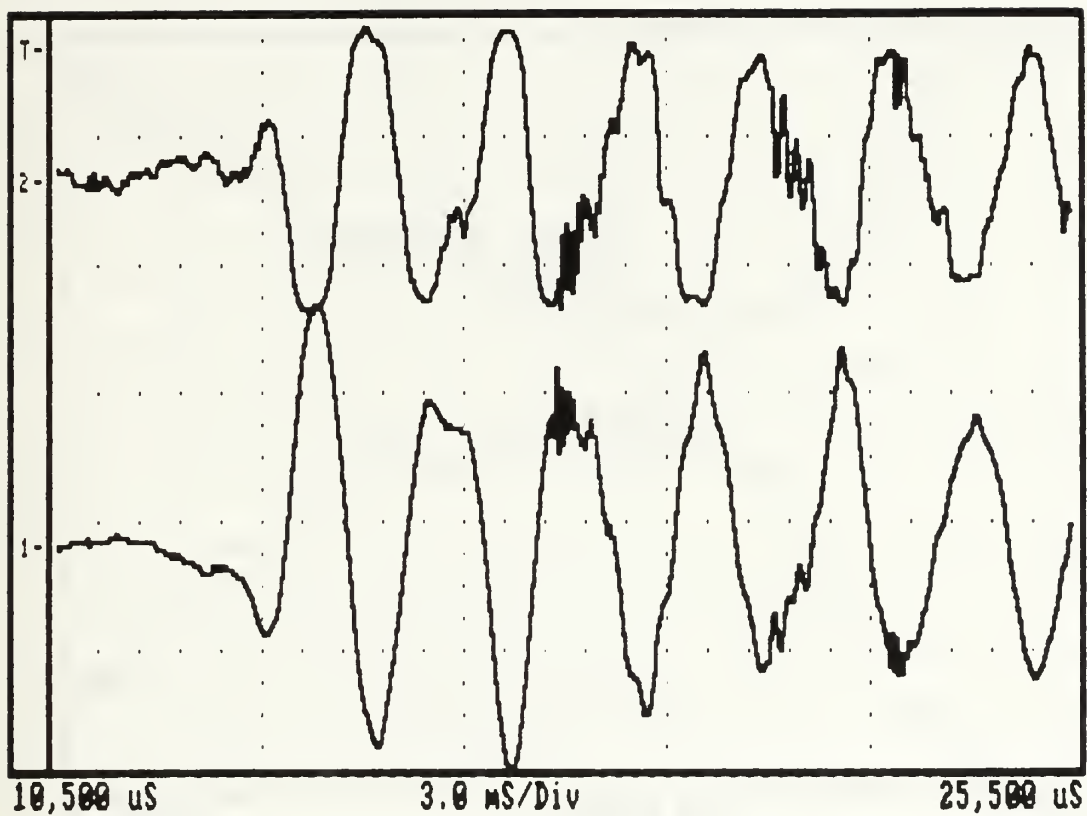
Figure 6. **Additional smaller bubble identification:** Several bubbles with higher frequency can be seen superimposed on the initial bubble signal. This is 15 ms of the 120 ms plotted in figure 5. Sampling period is 15 microseconds.

17
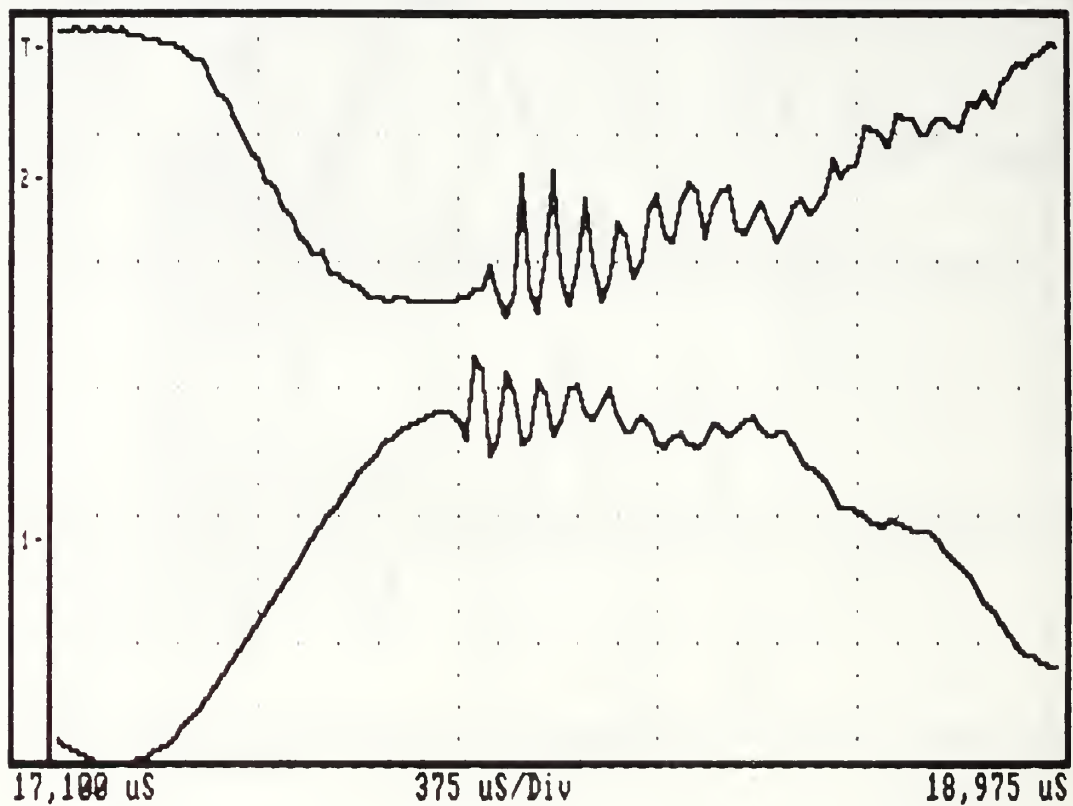
Figure 7. Small bubble identification: Frequency is 16.6 kHz. This is a 1.875 ms section of the signal shown in figure 5. Sampling period is 15 microseconds.

C. BUBBLE LOCATION

The location of the bubble can be determined using the geometry of the hydrophone positions and the relationships developed from the difference in time of arrival of the sound pressure wave to the hydrophones. In this procedure it was assumed that the bubbles were created and remain approximately at the surface of the water. The argument for this assumption follows: the bubbles were produced from the action of the breaking wave entraining pockets of air. This catastrophic force was the driving mechanism causing the oscillation. It was observed that the bubble oscillations only lasted for a short duration, of the order of tens of milliseconds, after the bubble formation. In this short period of action the bubble could not physically travel any significant distance.

A second assumption is that the surface of the water remained horizontal, ignoring the wave height. The error due to this assumption will be examined shortly.

When two hydrophones are placed in a vertical array the sound pressure wave from a bubble at the surface will arrive at the hydrophones at different times. This difference in time of arrival will be a function of the distance the wave must travel through the water.

Bubbles produced near the surface of the water act as dipole sources. The dipole consists of the bubble and an imaginary source the same distance above the surface as the bubble is below, with a distance L separating this image and the bubble. With the assumption that $kL < 1$, the dipole radiation pattern will be defined by the following equation from Morse and Ingard (1968):

$$P = (\frac{k^2}{4\pi R})\rho c D \cos(\theta)(1 + \frac{i}{kR})e^{i(wt-kR)}$$

where k is the wave number in radians/meter, R is the range in meters from the bubble to the hydrophone, ρc is the acoustic impedance of water in Pa sec/m, $D = VL$ where $V = 4\pi a^2 U$ is the volume per time, U is the radial velocity amplitude, θ is the angle between the axis of the dipole and the line adjoining the bubble and the hydrophone, and w is the angular frequency of the oscillating bubble in radians/second. The magnitude of the pressure at hydrophone 1 can be described as

$$| P_1 | = [k^2\rho c D \cos(\frac{\theta}{4\pi R_1})][1 + \frac{1}{k^2 R_1^2}]^{\frac{1}{2}}.$$

Using the relationship

$$a + ib = (a^2 + b^2)^{\frac{1}{2}} e^{i\theta}$$

so that the term

$$(1 + \frac{i}{kR}) = (1 + \frac{1}{k^2 R^2})^{\frac{1}{2}} e^{i\theta}$$

and

$$\theta = \tan^{-1}(\frac{b}{a}) = \tan^{-1}(\frac{1}{kR}).$$

The real part of the pressure at hydrophone 1 can now be described by the equation:

$$P_1 = |\, P_1 \,| \, Re(e^{i(wt - kR_1 + \theta)})$$

or restated

$$P_1 = |\, P_1 \,| \cos(wt_1 - kR_1 + \tan^{-1}(\frac{1}{kR_1})).$$

Identically, the real part of the pressure at hydrophone 2 can be written:

$$P_2 = |\, P_2 \,| \cos(wt_2 - kR_2 + \tan^{-1}(\frac{1}{kR_2})).$$

Comparing the phases for the times that the peaks occur,

$$wt_1 - kR_1 + \tan^{-1}(\frac{1}{kR_1}) = n\pi$$

and

$$wt_2 - kR_2 + \tan^{-1}(\frac{1}{kR_2}) = n\pi$$

and subtracting yields:

$$w(t_2 - t_1) - k(R_2 - R_1) + \tan^{-1}(\frac{1}{kR_2}) - \tan^{-1}(\frac{1}{kR_1}) = 0.$$

The equation describing the difference in time of arrival can be written as:

$$t_2 - t_1 = \left(\frac{R_2 - R_1}{c} \right) + \left(\frac{1}{2\pi f} \right) \tan^{-1}\left(\frac{1}{kR_1} \right) - \left(\frac{1}{2\pi f} \right) \tan^{-1}\left(\frac{1}{kR_2} \right)$$

where R_1 and R_2 are the distances from the bubble to the hydrophones in meters, k is the wave number in radians meter, c is the speed of sound in meters second, and f is the resonance frequency of the bubble in Hertz.

The geometry of the hydrophones is depicted in figure (8). The following relationships should be noted:

$$R_1 = (h_1^2 + x^2)^{\frac{1}{2}}$$

$$R_2 = (h_2^2 + x^2)^{\frac{1}{2}}$$

where h_1 and h_2 are the depths of the hydrophones in meters and x is the horizontal distance on the surface of the water above the hydrophone array in meters. If the position on the surface above the hydrophones is treated as an origin, x is in fact the radius of a circle. If these equations for R_1 and R_2 are placed in the previous equation for time of arrival difference, this radius, x, will remain the only unknown. Using an iterative program, the computer will easily determine the solution.

The position of the bubble on the surface can be determined by using two vertical arrays of hydrophones. The bubble will be located somewhere on the circles surrounding the arrays. These circles will intersect at two points, in a symmetrical manner about the horizontal line separating the arrays as in figure (9). The ambiguity between the two intersections is unimportant to the objectives of the experiment.

The fact that the surface of the water is not constantly horizontal, but in reality consists of various wave heights, causes a change in the time of arrival difference between the hydrophones of an array. If the bubble is located on a wave crest or trough the distance the pressure wave will have to travel can be described by:

$$R_1 = ((h_1 + \Delta h)^2 + x^2)^{\frac{1}{2}}$$

$$R_2 = ((h_2 + \Delta h)^2 + x^2)^{\frac{1}{2}}$$

where Δh is the vertical difference in bubble position from the horizontal surface of the water. This difference in time of arrival caused by the wave amplitude is shown in figure (10). It will be noted that the maximum amplitude of the waves in the tank is

approximately 3 cm. At this wave height the error in time of arrival is only 5 microseconds. Because of the fact that the wave height follows a Gaussian distribution, the wave height at the bubble location will likely be on the order of 1 cm and the error in time would be 2 microseconds with a corresponding error in bubble location of an insignificant 2 or 3 millimeters.

Two vertical arrays, each including a shallow hydrophone at 16 cm depth, and a deep hydrophone at 31 cm depth, were placed in the tank in the area where most waves break. The perpendicular line between the hydrophone arrays was set at approximately a 30 degree angle to the direction of the wave propogation in order to ensure geometric efficiency in the calculation of bubble positions. The buffer length was set to 100 milliseconds with a corresponding sampling period of 6 microseconds (spatial resolution, 9 mm). This small sampling period was considered necessary in order to measure the time of arrival difference as accurately as possible. The output went through the preamplifiers set at a gain of 5000 and acted as the trigger to the computerscope analog to digital converter.

The difference in time of arrival to the two vertical pairs of hydrophones, the resonance frequency of the bubble, and the time that the bubble began oscillating relative to the breaking of the wave, were recorded in the first 100 milliseconds for each bubble created by a breaking wave. This information was used with the iterative computer program to plot the locations of the individual bubbles. Figure (11) is the result of one breaking wave showing the symmetrical distribution of the bubbles created in the first 100 milliseconds after breaking. The symmetrical locations are caused by the two intersections of the bubble radii circles about the axes of the hydrophones. As long as the wave does not break close to the hydrophones it is not necessary to plot both sets of location positions because it is the relative positions of the bubbles that is necessary for density calculations. Figures (12) and (13) show the bubble locations with only the positive positions recorded.

The position plots demonstrate the bubble patches or "hot spots" often noted in acoustical measurements at sea. The plots were divided by a grid consisting of squares 5 cm on a side. These blocks of 25 square centimeters were used to calculate the area over which bubbles were produced. This large area assigned to any bubble counters and compensates for any error in the calculation of bubble position. Each square with a bubble in residence was counted. The average total area of bubble production was 345 square centimeters per breaking wave with a standard deviation of 42 square centimeters. It was assumed that all bubbles created by a breaker originate in such a calculated

22

area. It was not possible to expand the time of observation in order to confirm this assumption for later bubbles because the sampling period would also have become longer and the resolution of the time of arrival difference would not have been sufficient for accurate bubble location. Another method was to form a rectangle around the bubbles and compute the production area. The average production area calculated with this method was 320 square centimeters with a standard deviation of 96 square centimeters. The rectangle is marked by a solid line around the bubbles in figures (12) and (13). The two methods compare within 10 percent for the average production areas.

Another result of the bubble position plots was the ability to label the order in which the bubbles were created by the breaking wave. Figures (12) and (13) also show these relative positions of the bubbles from two waves each marked with the order in which they were produced. The order of the positions does not demonstrate that the location of the bubble depends on the relative time of its creation with respect to the breaking of the wave. The first bubble created was not necessarily the closest to the position where the wave breaks. Also the last bubble created was not necessarily located the farthest along the direction of wave propagation from the position where the wave began breaking. This fact suggests that the majority of the bubbles created were located within the area calculated even though this area was calculated from bubbles originating in the first 100 milliseconds of breaking.

Bubbles observed within the bubble location plots were ocassionally positioned in roughly linear patterns not necessarily perpendicular to the direction of wave propogation. The bubbles within these patterns all originate consecutively in short widows of time. It is believed that these bubbles are created by and along the small capillary waves which sometimes are seen superimposed on the face of a main wave. This evidence of capillary waves is examined in Appendix A.
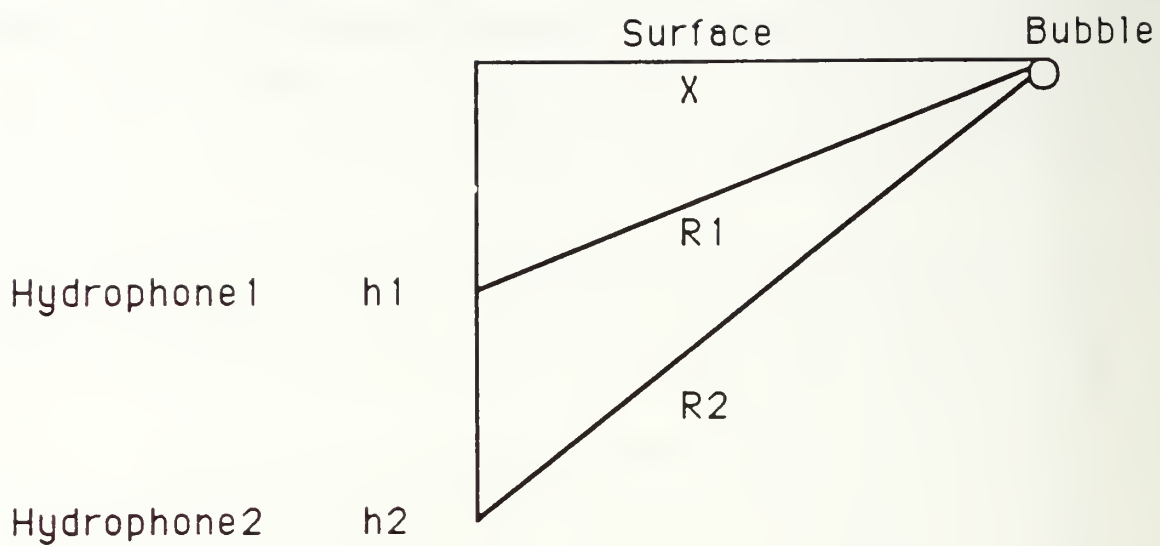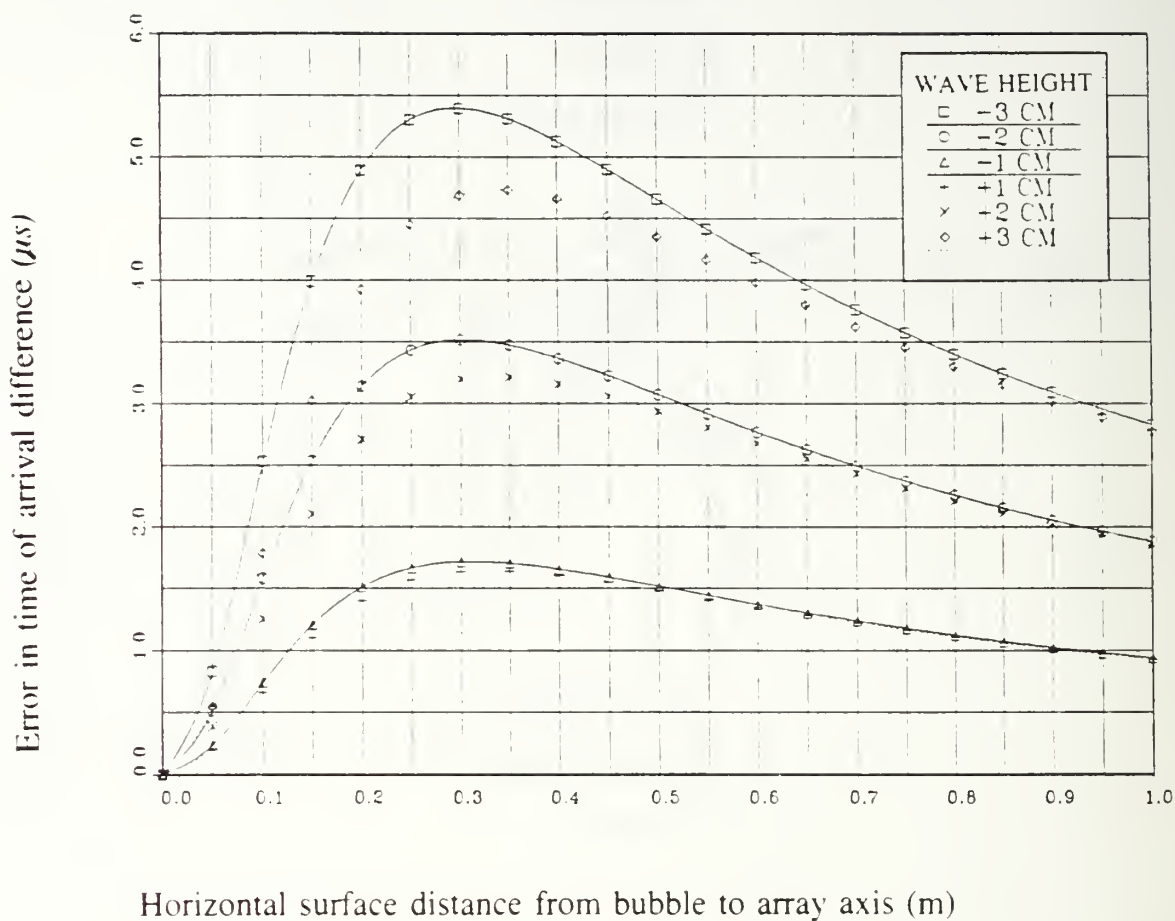
Figure 8. Bubble location geometry.

Possible
Bubble
Positions

x_1

x_2

h1   h1

h2   h2
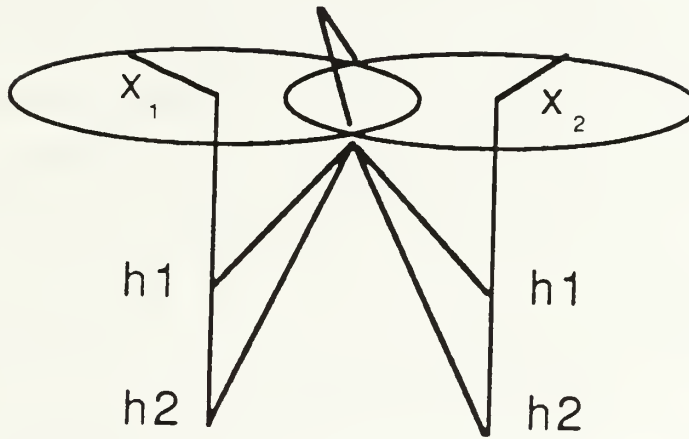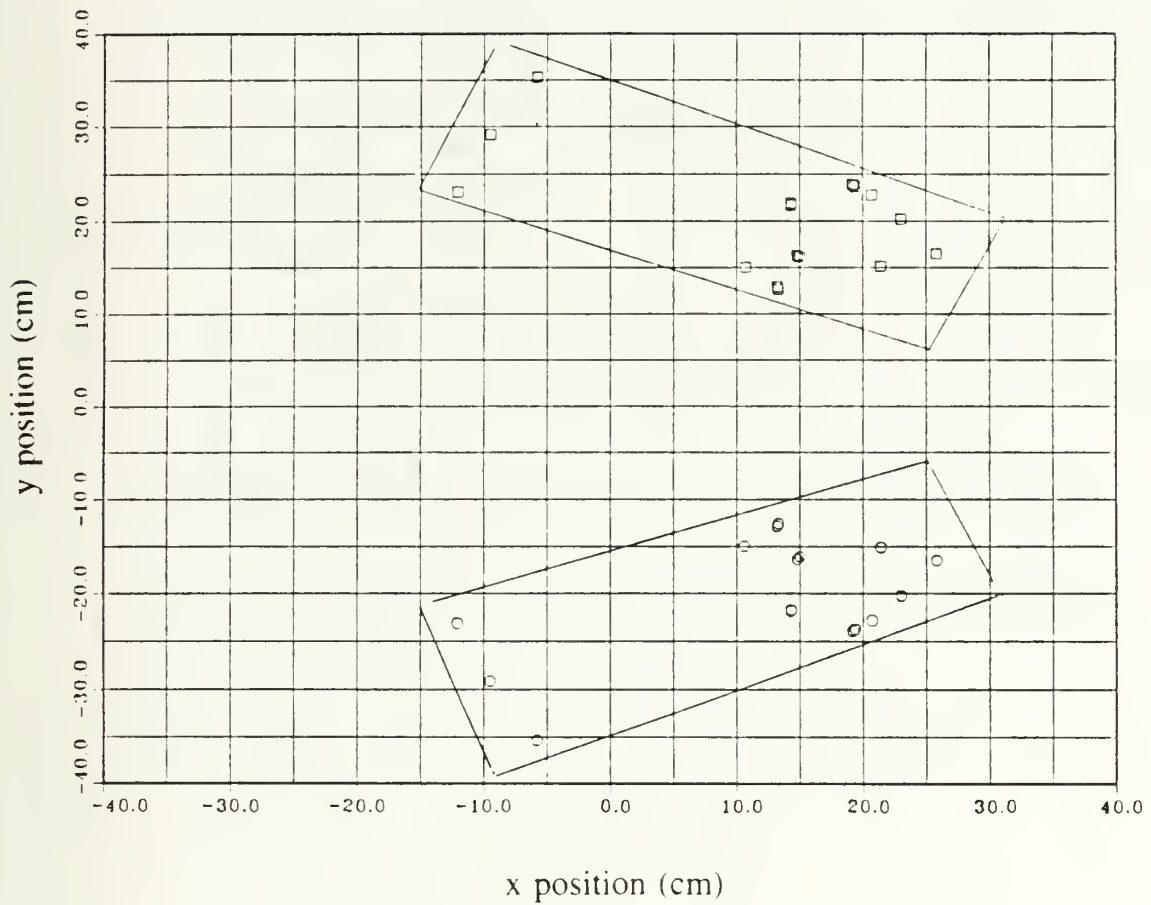
Vertical
Hydrophone
Arrays

Figure 9. **Bubble location technique:** Intersection of the two circles of radii x_1 and x_2 around the hydrophone axes marks the possible location of the bubbles.

Figure 10. Timing error due to wave height: Error in time of arrival caused by the additional distance traveled by the noise of a bubble on the surface of the water due to local wave height above mean surface.

Figure 11. Distribution of bubble locations: Distribution is symmetric about the line joining the two vertical arrays. Bubbles are from the first 100 ms after the breaking of the wave.
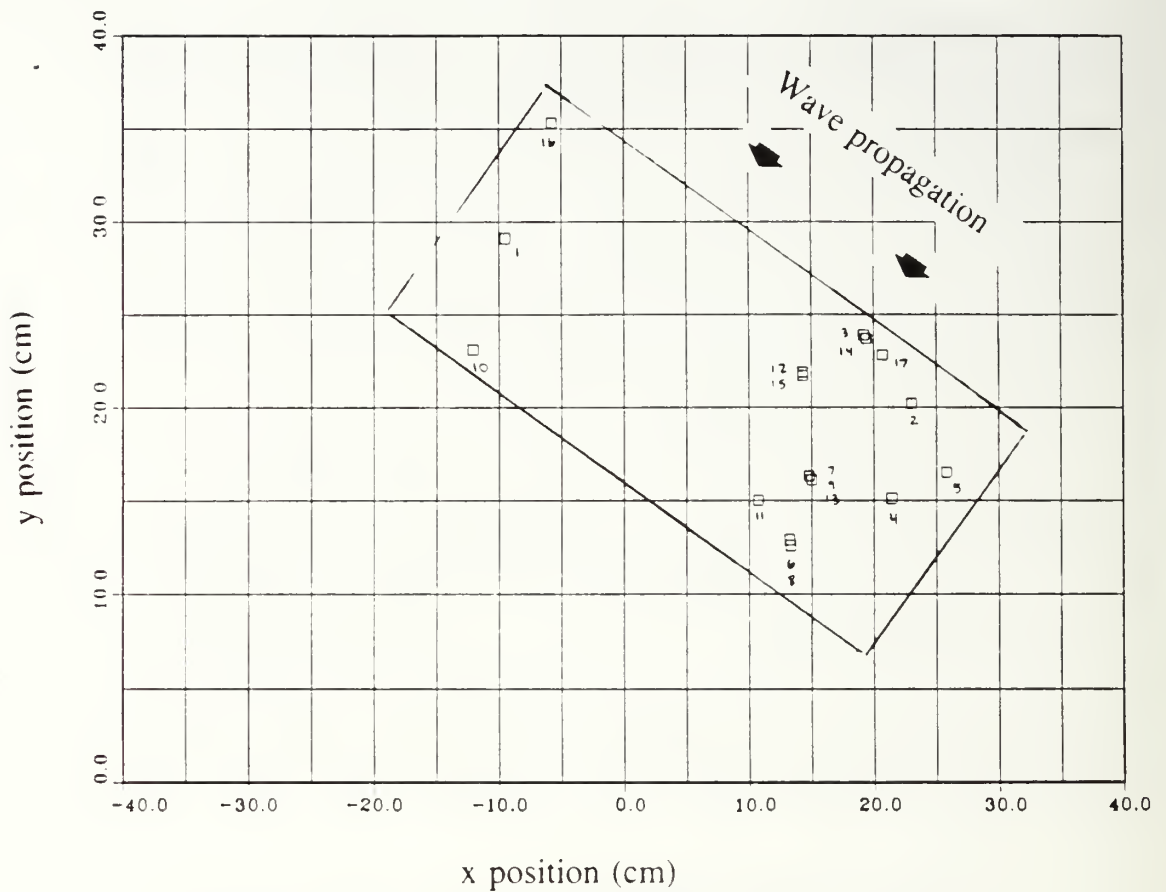
Figure 12. Bubble location plot: Bubble locations marked with the order of bubble creation. Same breaker as figure 11. Bubbles are from the first 100 ms after the breaking of the wave.

28
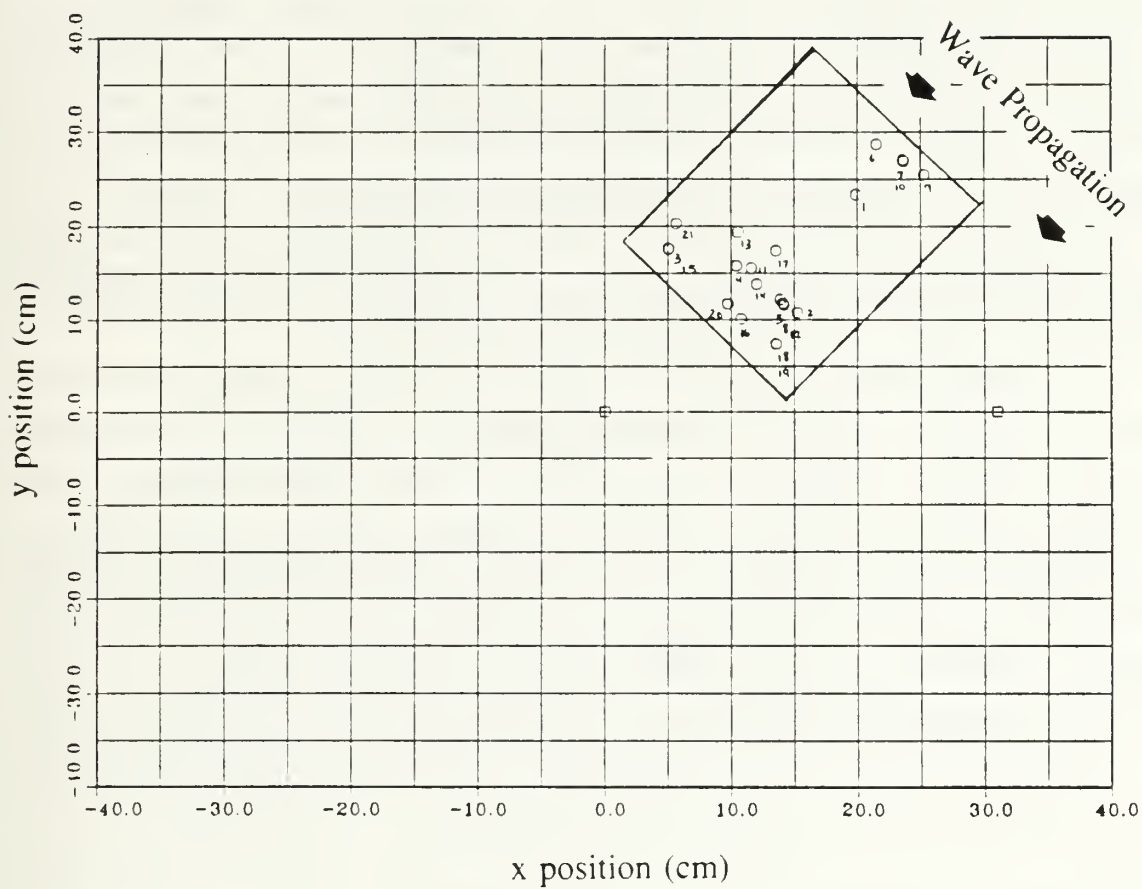
Figure 13. Bubble location plot: Bubble locations marked with the order of bubble creation. Bubbles are from the first 100 ms after the breaking of the wave.

D. RATE OF BUBBLE PRODUCTION

It was observed from the use of the Hewlett-Packard 3561A Spectrum Analyzer that noise is produced from a breaking wave for a period of 2 to 3 seconds after the first sound of a breaking wave is heard. The digital processing equipment used to identify, locate, and count bubbles has a relatively small memory (64k bites). This does not permit the sound to be captured for a long enough period of time to record all bubbles produced and simultaneously have a sampling period small enogh to be of use in the identification of bubble resonance frequencies. Therefore it was thus necessary to determine the rate at which bubbles are produced over time in order to determine an expression defining the bubble production rate relative to the time at which the wave breaks. The measurements could then be made for shorter periods of time and then extrapolated to determine the total number of bubbles produced.

Two omnidirectional hydrophones were placed in a vertical array in the tank at depths of 12 and 24 centimeters. The buffer length for two hydrophones was expanded to 500 milliseconds by using a sampling period of 15 microseconds. Through experimentation and consideration of the Nyquist relationship it was determined that this was the maximum sampling period that would allow dependable identification of bubbles with resonance frequencies less than 33 kHz. The trigger level was adjusted to a level sufficiently high to ensure the sampling equipment would begin capture only when a wave was breaking almost directly above the hydrophones. This was done to guarantee the observation of bubbles with a small amplitude which may not have been seen from a longer distance and at a greater angle from the dipole. The short range from the hydrophones can be confirmed using the method previously described. The input signal passed through the preamplifier with the gain set on 5000. A total of 10 breaking waves were observed.

The average number of bubbles of all radii produced per breaker, within time increments of 10 milliseconds, is plotted against the time after the breaking of the wave in figure (14). Additionally, the production rates for bubbles with bubble radii broken down into bands of greater than 2.2 mm (resonance frequency less than 1500 Hz), between 2.2 mm (1500 Hz) and 0.16 mm (20 kHz), and less than 0.16 mm (greater than 20 kHz), are depicted in figures (15), (16), and (17) respectively. These bands are chosen to accentuate the bubble production behavior in the Knudsen sea noise spectrum frequency regime generally taken to be between 500 Hz and 20 kHz.

The production spectrum of the two radii bands, 0.16 to 2.2 mm and smaller than 0.16 mm as seen in figures (16) and (17), suggests that bubbles in these bands are

produced with an exponential rate of decrease. The equations which approximate the decay rates for these two bands are:

$$\frac{dN}{dt} = 0.311e^{-.0127t}$$

and

$$\frac{dN}{dt} = 0.127e^{-.0093t}$$

respectively. This is probably also true for the largest bubbles but not enough data is available to show it.

The curve which best approximates the exponentially declining total production rate of figure (14) is:

$$\frac{dN}{dt} = 0.313e^{-.0070t}$$

where dN/dt is the number of bubbles produced per millisecond and t is time after the breaking of the wave in milliseconds. The expression stated above can be integrated to describe the bubble production rate out to specified times. When the integration was performed to infinity it was found that less than 0.1 percent of the bubbles would originate after the first second. About 97 percent of the bubbles were formed in the first 500 milliseconds after the wave breaks.
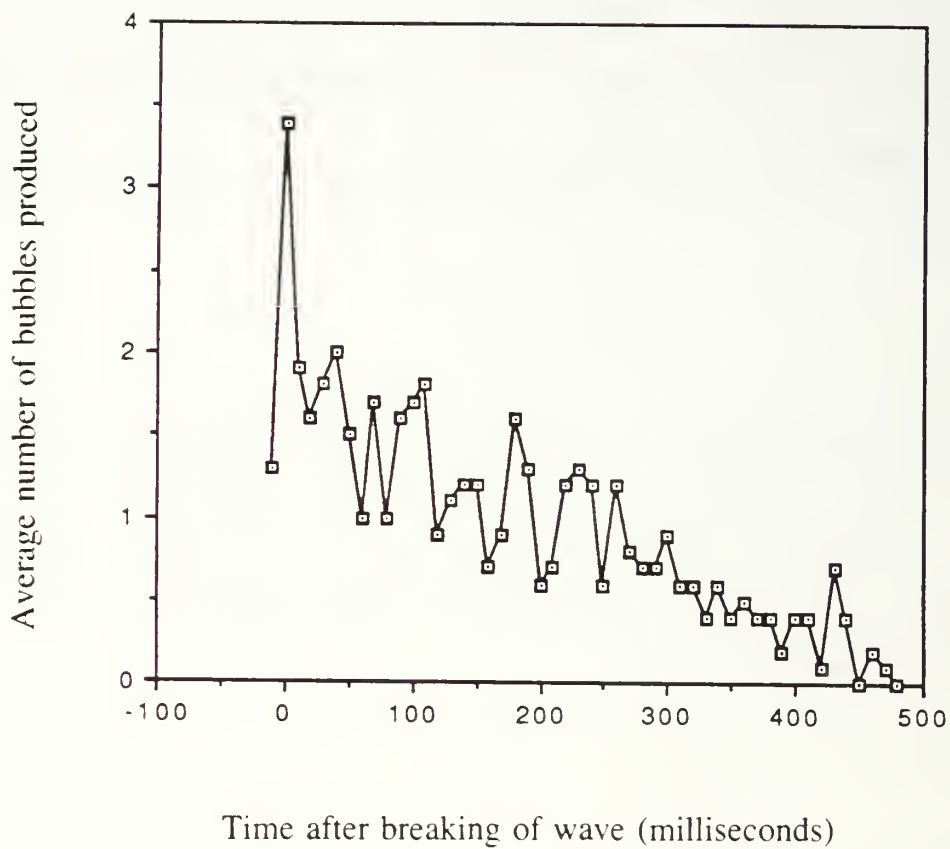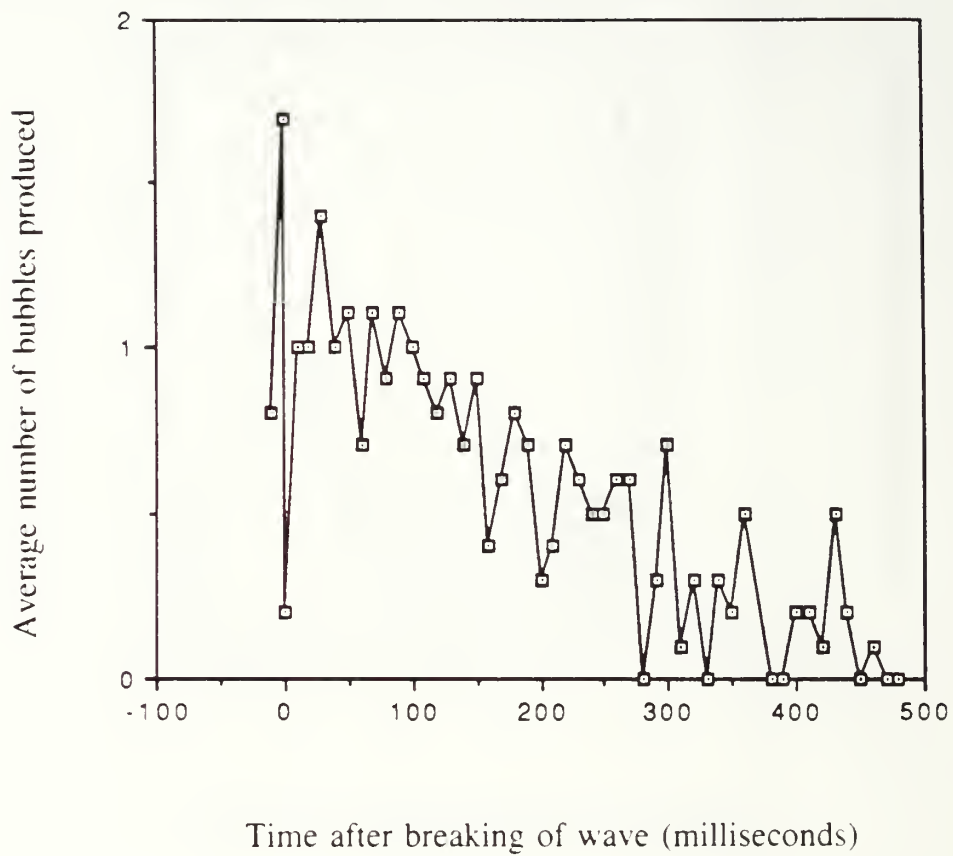
Figure 14. Average number of bubbles produced per laboratory breaker: (all sizes). The bubbles are counted within 10 ms increments.
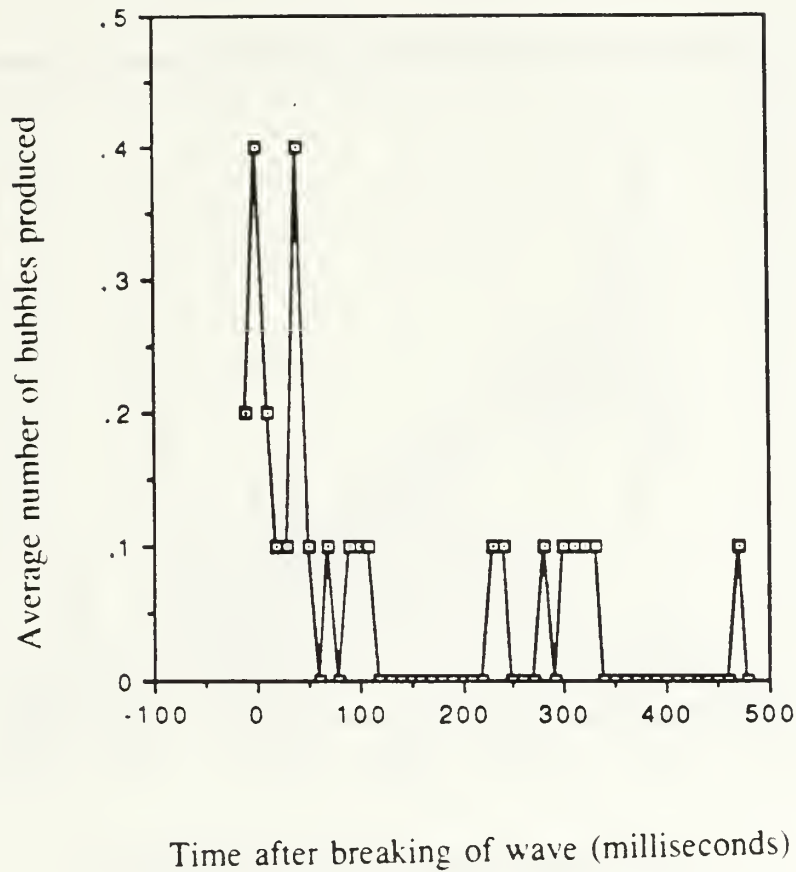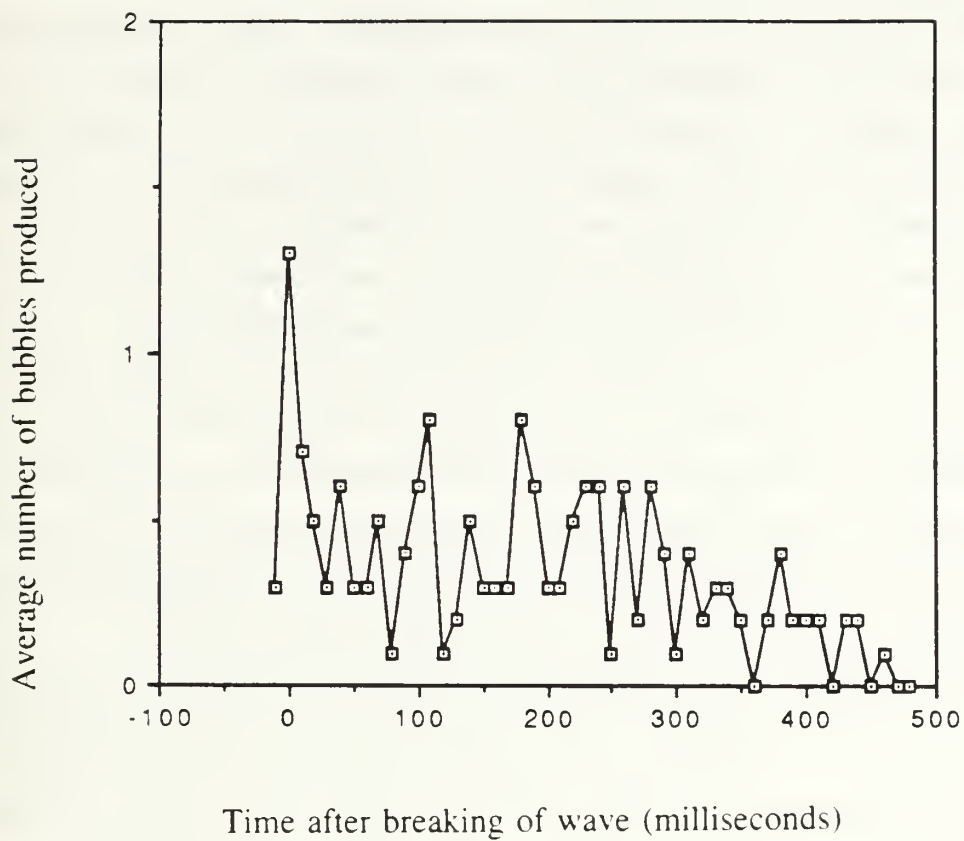
Figure 15. Average number of large bubbles per laboratory breaker: (radius >
2.2 mm). The bubbles are counted within 10 ms increments.

Figure 16. Average number of mid-size bubbles per laboratory breaker: (0.16 mm < radius < 2.2 mm). The bubbles are counted within 10 ms increments.

Figure 17. Average number of small bubbles per laborat~~ory~~ breaker: (radius ‹ 0.16 mm). The bubbles are counted within 10 m~~s~~ increments.

E. BUBBLE PRODUCTION DENSITY

The rate at which bubbles will be produced is related to the foam coverage. With this knowledge researchers will be better able to understand the phenomena which affect acoustics, weather, aerosol production, and any other sea surface interactions. The two major requirements for density calculations have already been covered: the bubble creation rate relative to the start of the breaking of the wave, and the area over which these bubbles are being produced.

All bubbles in figures (15) - (17) with equal radii were summed and the average number of bubbles per breaker with that radius was computed by dividing by the number of waves observed. In an earlier experiment it was found that only 3 percent more bubbles originated in the second 500 milliseconds after the breaking of the wave. Because the measurements were again taken over a period of 500 milliseconds the number of bubbles observed was thus increased by 3 percent to give the number of bubbles in the first second. This number is now defined as the "total" number of bubbles. In an additional earlier experiment it was found that the average area of bubble production spanned 345 square centimeters or equivalently 0.0345 square meters. The "total" number of bubbles was divided by 0.0345 to give the resulting average bubble production density in bubbles per square meter for each bubble radius observed. Thus the bubble production will be expressed in bubbles per square meter and assumes negligible numbers of bubbles are formed beyond the first second after the wave breaks.

Bubbles were observed with finite numbers of different size radii. If an infinite number of waves were measured, eventually bubbles would be observed having every possible radius up to the maximum gas volume that can physically be encapsulated. To account for this limitation in the data recorded, the span in bubble radius in microns was calculated to include half the bubble radius size between each of the subsequent smaller and larger bubble observations. The number of bubbles per square meter was divided by this radius span to give the bubble density in bubbles per square meter per micron of bubble radius increment.

The bubble production density is plotted on semilog paper with the radius on a logarithmic scale in figure (18), and both bubble radius and density on a logarithmic scale in figure (19). It can be seen that the most commonly produced bubble was 0.15 mm in radius produced at the approximate density of 5.9 bubbles per square meter per micron radius increment. The smallest bubble radius measured was 0.048 mm which has a corresponding resonance frequency of 66 kHz. The largest bubble was of radius 7.4

mm with a corresponding resonance frequency of 440 Hz. It will be assumed that still larger bubbles would not have been found even if more breakers had been observed.

Once the production density of bubbles for each radius has been calculated the volume of gas encapsulated from each known bubble radius can be computed. Figure (20) is a summary of cubic centimeters of gas volume encapsulated per square meter of breaking wave for bubbles of various radii. Although it was seen in figures (18) and (19) that the majority of bubbles produced were less than 0.5 mm in radius, the contribution to total gas entrainment from these small bubbles is minimal. Assuming that there are no bubbles larger than the largest measured in 10 breakers which had a radius of 7.4 mm, the individual contributions from each bubble radius can be summed to give a volume rate of gas encapsulation which averages 23 cubic centimeters of gas encapsulated per square meter of breaking wave in the laboratory. More than half of this total volume came from bubbles with radius greater than 3 millimeters.
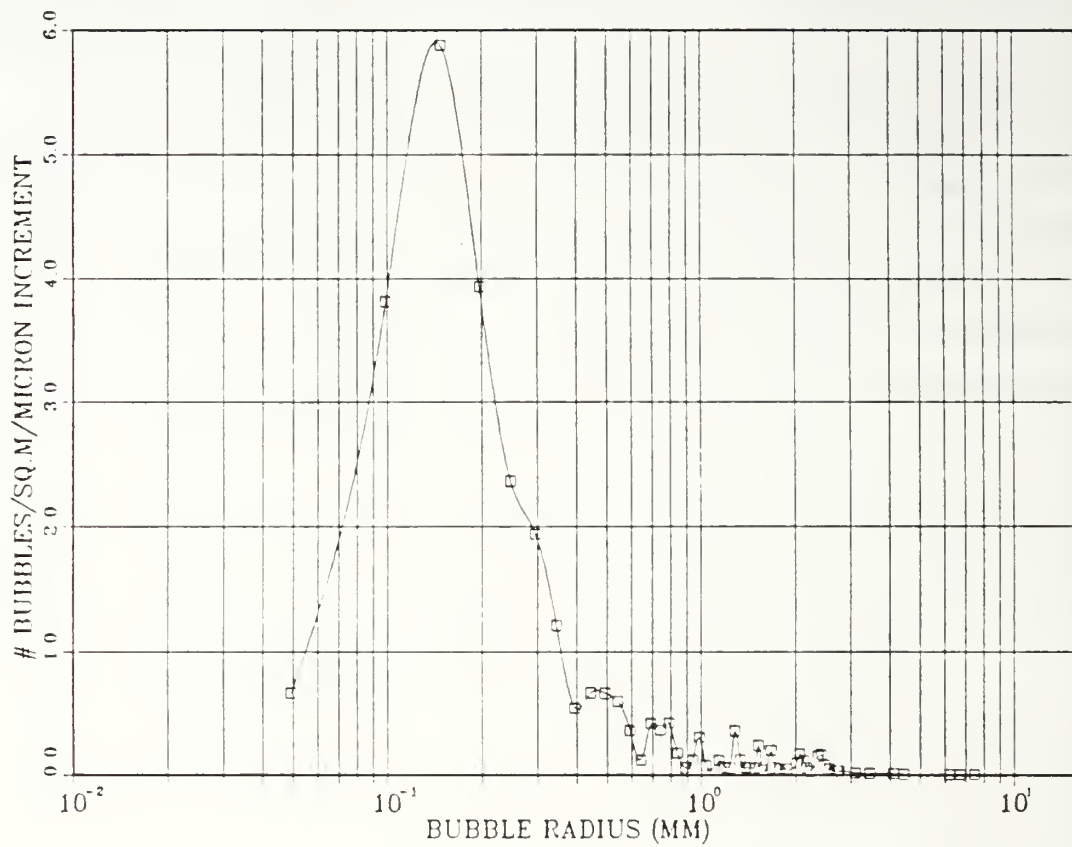
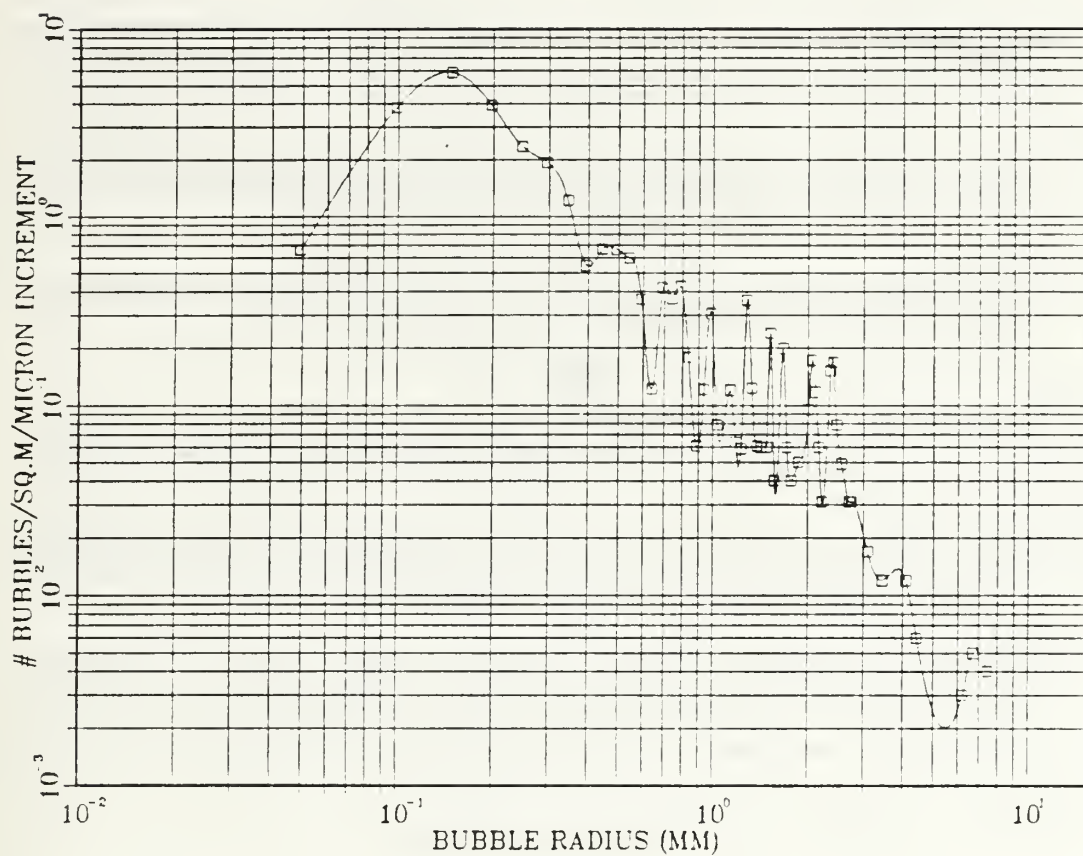Figure 18. Average surface density of bubbles produced.

38

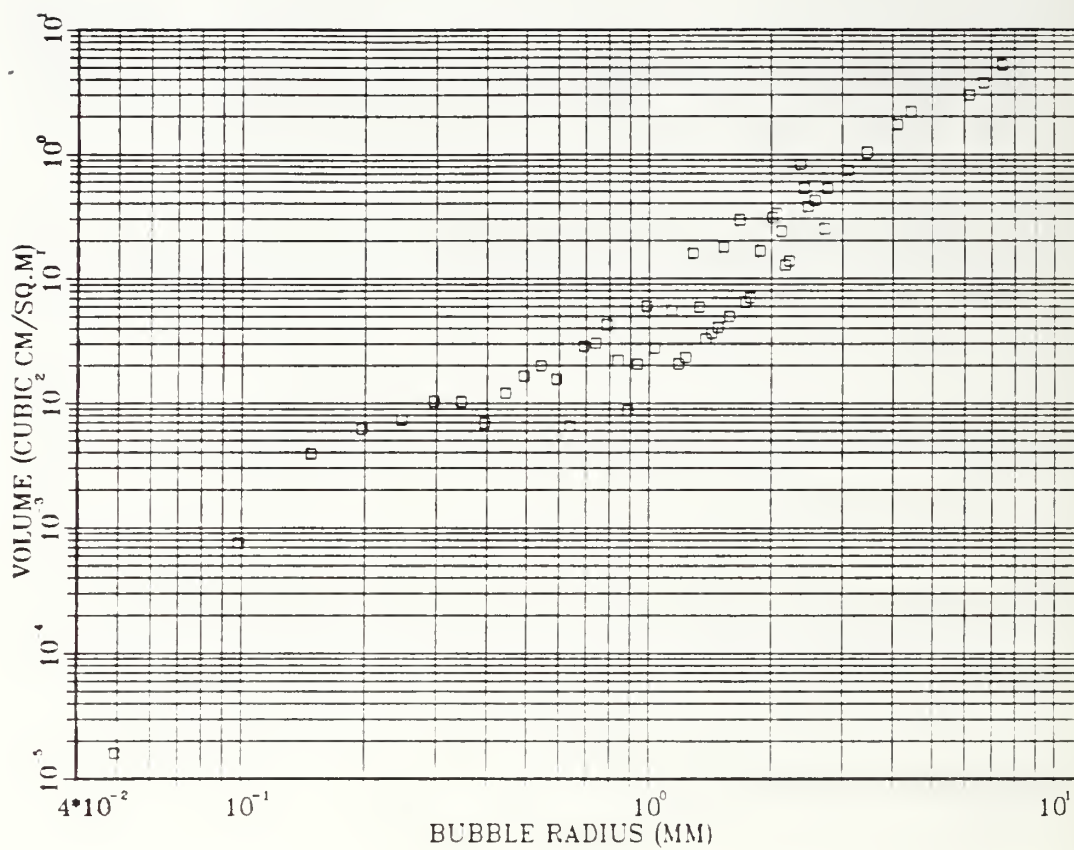Figure 19. Average surface density of bubbles produced.

Figure 20. Volume of air encapsulation per surface area.

40

V.   COMPARISON WITH OTHER DETERMINATIONS

We know of only one other attempt to measure the bubble production in a spilling breaker, that was by Toba (1961). Contrary to our breakers being produced by an oscillating wedge with no wind, Toba used wind of different speeds and fetch in a flume. Toba's method considered that an equilibrium existed between the bubbles entering from periodic breaking at the water surface and those rising to the surface. His photographs were made of the volume density of bubbles, not the surface production density of the bubbles which is our goal. He used the time between breakers to infer the bubble encapsulation rate using the relationship

$$\beta = \left(\frac{\alpha}{100} \right) \frac{\Theta}{T}$$

where β is the bubble encapsulation rate in bubbles/square cm second, $\frac{\alpha}{100}$ is the percentage of crests actually entraining bubbles, Θ is the total number of bubbles of a particular size in a water column of unit base area, and T is the period of the main surface wave. The shape of Toba's encapsulation spectrum, figures (21) and (22), was very similar to that in this experiment with a sharp peak at a single bubble radius. However the peak of Toba's bubble production was at approximately 0.38 mm in radius at a rate of approximately 0.2 bubbles per square centimeter per second for a wind speed 12.1 m/sec. His photographic measurements included 6 different sizes of bubbles with radii from 0.15 mm to 6.0 mm. Our method observed 53 bubble radii from 0.048 mm to 7.4 mm. His smallest radius bubble was our most common bubble. The production rate inferred by Toba for 12.1 m sec wind was of the same order as the rate measured directly acoustically.

There have been extensive measurements of the foam coverage at sea using aerial photography and satellite imaging. The foam coverage is a measurement of residual bubbles including those convected upward from below and lacking those that have been convected from the surface to lower depths or that have burst at the surface. Thus the area of coverage can not be used directly with the densities measured in this experiment to calculate the bubble populations beneath the ocean surface. Further experimentation is required in order to understand exactly what is being measured from the foam of breaking waves.
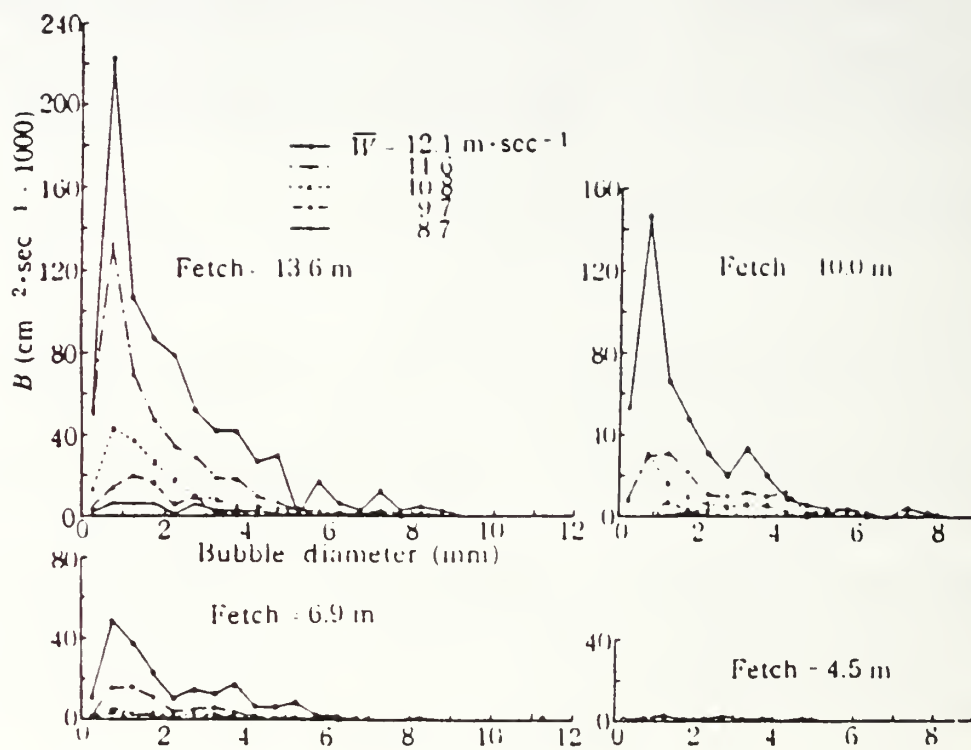
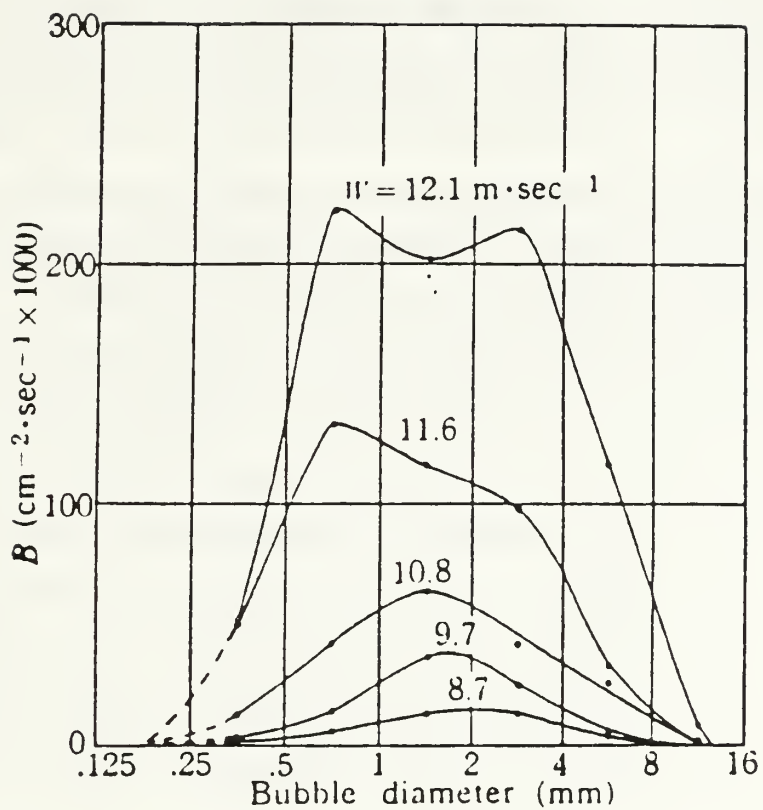Figure 21. Rate of formation of air bubbles in wind waves (Toba).

Figure 22. Rate of formation of air bubbles in wind waves (Toba): plotted per equal log (bubble size) interval.

VI. CONCLUSIONS

The method described throughout this thesis achieved its goal of obtaining the bubble production density from plunger generated spilling breakers. The technique used was to passively observe the amplitude and frequency of the randomly pulsed sound emitted by the breakers. The results give more details of the characteristics of bubble production than previous experimental techniques used for obtaining surface bubble densities.

Bubbles were positively identified throughout a radius range of 0.048 to 7.4 millimeters. Most of the bubbles originate in the first 500 milliseconds after the breaking of the wave though sound from bubbles has been recorded for a period of 2 to 3 seconds after breaking. The bubbles were produced with an exponentially decreasing rate following a decay constant of -0.007t with time measured in milliseconds after the breaking of the wave. The average area of bubble production from breaking waves in the tank was 345 square centimeters. The most commonly produced bubble had a radius of 0.15 millimeters and was entrained at a density of 5.9 bubbles per square meter per micron of bubble radius increment. This bubble radius is smaller than the minimum bubble radius measured in other experiments using photographic techniques to obtain bubble volume density. The greater resolution using acoustics instead of photography has allowed 10 times the resolution in bubble radii identification for bubbles with radii between 0.25 and 2.0 millimeters. The average encapsulation of gas was 23 cubic centimeters per square meter of breaking wave.

Using the Knudsen sound radiated from the breaking waves as our sole criterion, whitecaps from spilling ocean waves have little physical difference from the breaking waves produced in the laboratory. If this is the case, the measurements reported here are useable for the ocean. The use of this passive acoustical technique in actual sea measurements may also be possible. If these laboratory data are confirmed by actual measurements of surface bubble production density at sea, and after further studies of bubble dissipation in a turbulent ocean, satellite measurements of the foam coverage from whitecaps could yield an estimate of the rate of bubble production in the ocean.
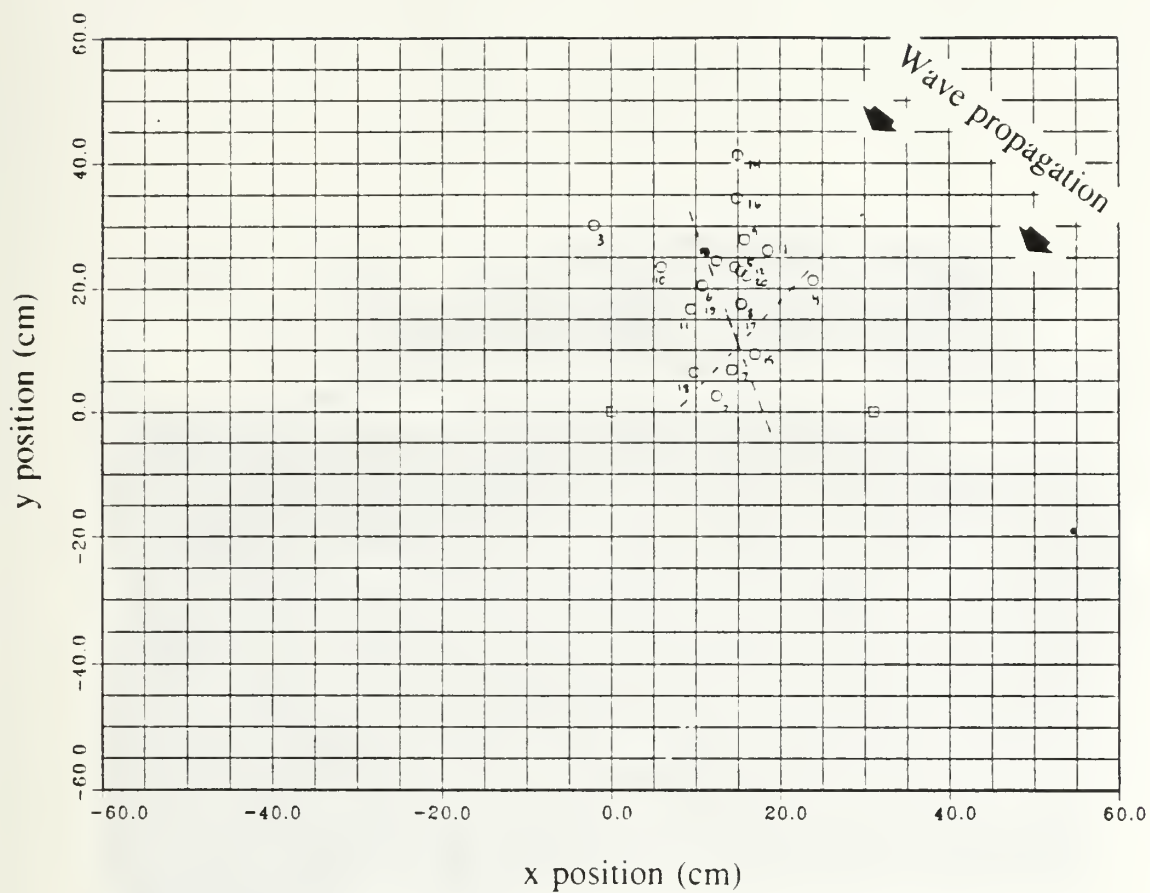
APPENDIX A. EVIDENCE OF CAPILLARY WAVES

Upon examination of the bubble location plots it was discovered that in some of the plots the bubbles appeared to be located along lines perpedicular to the wave propagation direction (fig 12) and in other cases the lines are not perpendicular to the direction of wave propagation. These lines appeared with varying angles ranging from 30 to 90 degrees away from the propagation direction. It was hypothesized that these may have been capillary waves forming on the face of the main wave. A purely arbitrary reference time of 10 milliseconds was chosen as the time within which all of the bubbles on the line must have originated. Figure (23) is an example of a capillary line identification. The bubbles were captured with a sampling period of 6 microseconds during the first 100 milliseconds after the wave broke. The order of bubble formation is marked on the figure and the following are the times of the beginning of the individual bubble oscillations after the breaking of the wave:

Bubble number	Origin time (ms)
1	2.92
2	5.88
3	10.56
4	11.22
5	12.44
6	18.74
7	20.54
8	24.99
9	31.15
10	33.66
11	42.37
12	42.49
13	49.03
14	56.52
15	69.30
16	75.23
17	78.65

45

18	80.45
19	81.83
20	93.94

The capillary lines on figure (23) are identified by bubbles 6 through 8 and by bubbles 17 through 19. Figures (24) and (25) are photographs of breaking waves in which the capillary waves may be clearly observed.

Figure 23. Possible capillary wave positions by bubble location: Lines are from bubbles 6-8 and 17-19.

·6
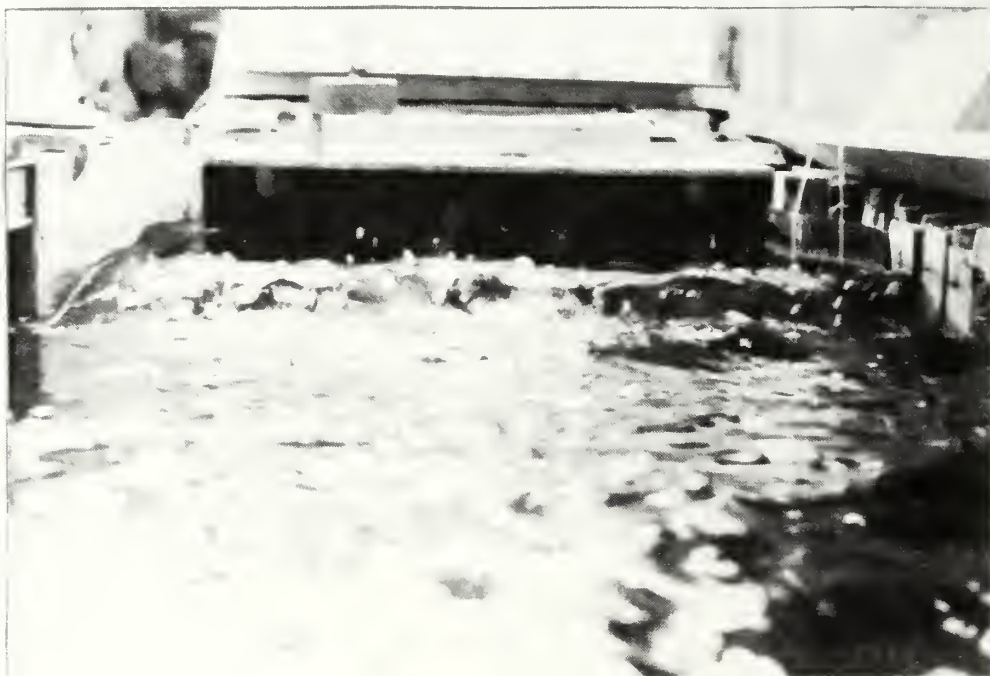
Figure 24. Photograph of capillary waves.

48

Figure 25. Photograph of capillary waves.

APPENDIX B.   VOLTAGE AMPLIFIERS

When receiving signals from many hydrophones simultaneously, it was necessary to develop a substitute for the limited number of Ithaco 1201 Preamplifiers. A series of preamplifiers was built using two 356 operational amplifiers in series with the necessary feedback elements. Figure (26) is the diagram of the amplifier circuit. Figure (27) shows the operational characteristics of the amplifier.
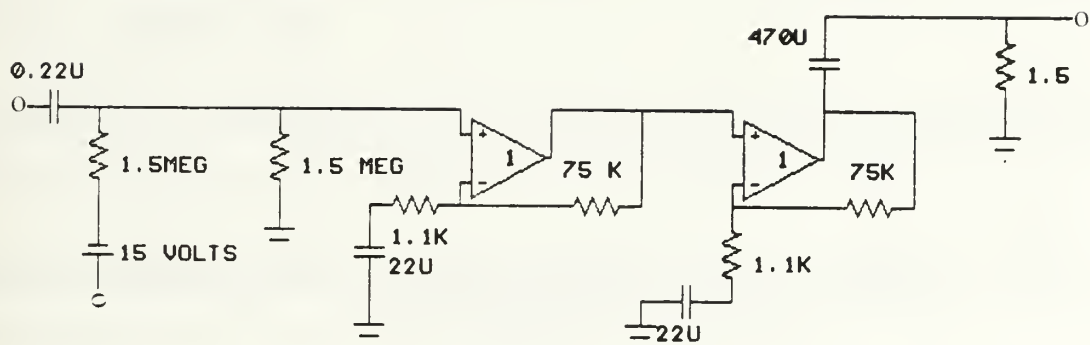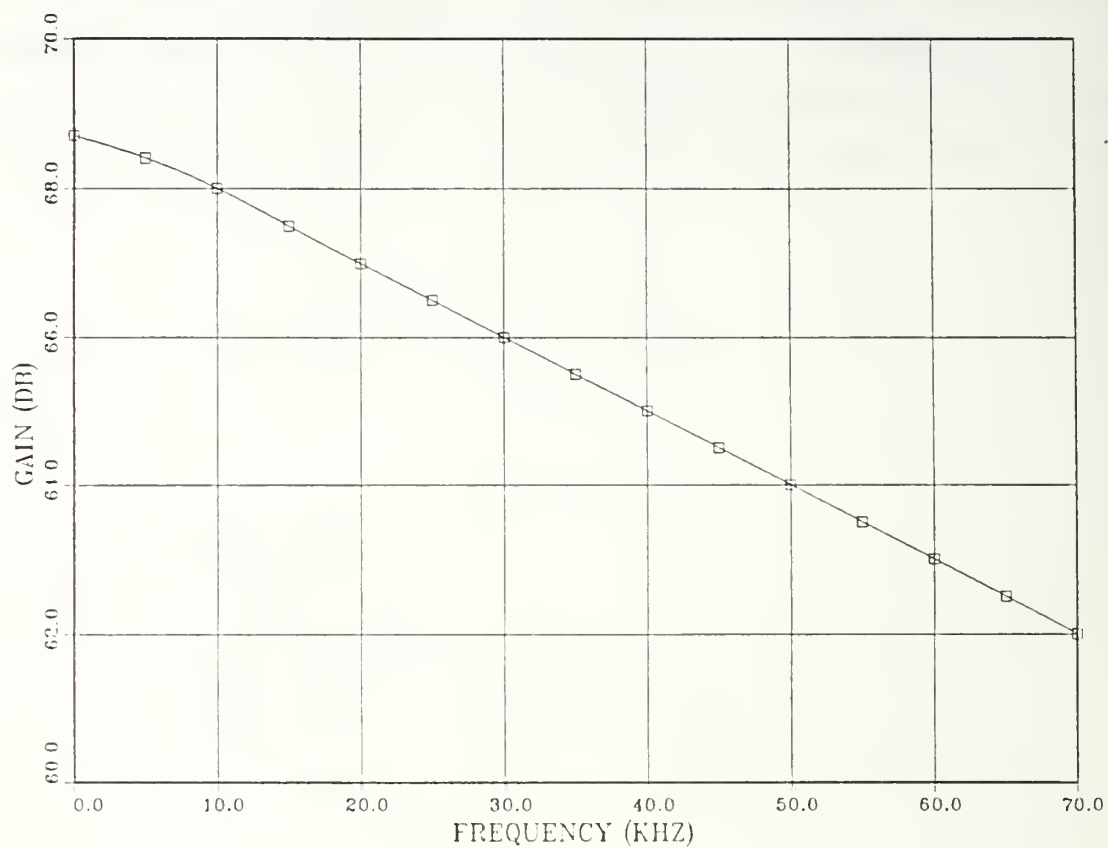
Figure 26. Amplifier circuit diagram.

51

Figure 27. Operational characteristics of the amplifier.

LIST OF REFERENCES

Breitz, N., and Medwin, H., "Instrumentation for in situ Acoustical Measurements of Bubble Spectra under Breaking Waves," *J. Acoust. Soc. Am.*, v. 86 pp. 739-743, 1989.

Clay, C.S., and Medwin, H., *Acoustical Oceanography: Principles and Applications*, John Wiley and Sons, New York, p. 196, 1977.

Farmer, D. M., and Vagle, S., "Waveguide propagation of ambient sound in the ocean-surface bubble layer," *J. Acoust. Soc. Am.*, v. 86 pp. 1897-1908, 1989.

Guchinski, H., "Bubble Coalescence in Sea and Freshwater: Requisites for an Explanation," E.C. Monahan and G. Mac Niocaill (Eds.), *Ocean Whitecaps*, p. 270, D. Reidel Publishing Company, 1986.

Holthuijsen, L. H., and Herbers, T. H. C., "Statistics of Breaking Waves Observed as Whitecaps in the Open Sea," *J. Phys. Ocean.*, v. 16 pp. 290-297, 1986.

Johnson, B. D., and Cooke, R. C., "Bubble Populations in Coastal Waters: A Photographic Approach," *J. Geophys. Res.*, v. 84 pp. 3761-3766, 1979.

Kolovayev, D. A., "Investigation of the Concentration and Statistical Size Distribution of Wind-Produced Bubbles in the Near-Surface Ocean," *Oceanology*, v. 15 pp. 659-661, 1976.

Levich, V. G., *Physiochemical Hydrodynamics*, Prentice Hall, 1962.

Longuet-Higgins, M. S., "Bubble Noise Spectra," *J. Acoust. Soc. Am.*, (submitted), 1989.

Medwin, H., and Beaky, M. M., "Bubble Sources of the Knudsen Sea Noise Spectra," *J. Acoust. Soc. Am.*, v. 86 pp. 1124-1130, 1989.

Miller, R. L., University of Chicago, Fluid Dynamics and Sediments Transport Laboratory, Dept. of Geophysical Sciences, Technical Report No. 13, 1972.

Morse, P. M., and Ingard, K. U., *Theoretical Acoustics*, McGraw-Hill, New York, 1968.

Toba, Y., and Koga, K., "A Parameter Describing Overall Conditions of Wave Breaking, Whitecapping, Sea-Spray Production, and Wind Stress," E. C. Monahan and G. Mac Niocaill (Eds.), *Ocean Whitecaps*, pp. 37-47, D. Reidell Publishing Company, 1986.

Toba, Y., "Drop Production by Bursting of Air Bubbles on the Sea Surface (III) Study by Use of a Wind Flume," *Memoirs of the College of Science*, University of Kyoto, Series A, v. XXIX, No. 3, Art. 4, pp. 313-344, 1961.

Thorpe, S. A., "Bubble Clouds: A Review of Their Detection by Sonar, of Related Models, and of How K_c may be Determined," E. C. Monahan and G. Mac Niocaill (Eds.), *Ocean Whitecaps*, pp. 57-68, D. Reidell Publishing Company, 1986.

Thorpe, S. A., and Hall, A. J., "The Characteristics of Breaking Waves, Bubble Clouds, and Near-Surface Currents Observed Using Side-Scan Sonar," *Continental Shelf Research*, v. 1 pp. 353-384, 1983.

Urick, R. J., *Principles of Underwater Sound*, 3rd Edition, McGraw-Hill Book Company, 1983.

INITIAL DISTRIBUTION LIST

No. Copies

1. Defense Technical Information Center   2
   Cameron Station
   Alexandria, VA 22304-6145

2. Library, Code 0142   2
   Naval Postgraduate School
   Monterey, CA 93943-5002

3. Prof H. Medwin (Code 61Md)   6
   Department of Physics
   Naval Postgraduate School
   Monterey, CA 93943-5004

4. Prof J. A. Nystuen   2
   Department of Oceanography
   Naval Postgraduate School
   Monterey, CA 93943-5004

5. Commanding Officer   3
   Attn: LT A. C. Daniel
   USS Deyo (DD-989)
   FPO Miami, FL 34090-1227

6. Office of Naval Research   1
   Attn: Dr. Marshall Orr
   800 N. Quincy
   Arlington, VA 22217

7. Prof A. A. Atchley   1
   Department of Physics
   Naval Postgraduate School
   Monterey, CA 93943-5004

8. David M. Farmer   1
   Institute of Ocean Sciences
   P. O. Box 6000
   Sidney, British Columbia, V8L4B2
   Canada

9. M. S. Longuet-Higgins   1
   Center for Studies of Nonlinear Dynamics
   La Jolla Institute
   7855 Fay Avenue, Suite 320
   La Jolla, CA 92037

10. S. A. Thorpe
    Institute of Oceanographic Sciences
    Wormley, Godalming, Surrey GU85UB
    United Kingdom

11. E. C. Monohan
    Marine Sciences Institute
    University of Connecticut
    Avery Point
    Groton, CT 06340

615-584

10. S. A. Thorpe
Institute of Oceanographic Sciences
Wormley, Godalming, Surrey GU8 5UB
United Kingdom

11. E. C. Monahan
Marine Sciences Institute
University of Connecticut
Avery Point
Groton, CT 06340